

Influence of Synoptic Weather Patterns on Solar Irradiance Variability in Northern Europe

KAJSA M. PARDING

Norwegian Meteorological Institute, Oslo, Norway

BEATE G. LIEPERT

NorthWest Research Associates, Redmond, Washington

LAURA M. HINKELMAN AND THOMAS P. ACKERMAN

*Joint Institute for the Study of Ocean and Atmosphere, University of Washington,
Seattle, Washington*

KNUT-FRODE DAGESTAD

Norwegian Meteorological Institute, Bergen, Norway


JAN ASLE OLSETH


Geophysical Institute, University of Bergen, Bergen, Norway

(Manuscript received 23 June 2015, in final form 12 January 2016)

ABSTRACT

Observations have revealed strong variability of shortwave (SW) irradiance at Earth's surface on decadal time scales, referred to as global dimming and brightening. Previous studies have attributed the dimming and brightening to changes in clouds and atmospheric aerosols. This study assesses the influence of atmospheric circulation on clouds and SW irradiance to separate the influence of "natural" SW variability from direct and, to some extent, indirect aerosol effects. The focus is on SW irradiance in northern Europe in summer and spring because there is little high-latitude SW irradiance during winter. As a measure of large-scale circulation the *Grosswetterlagen* (GWL) dataset, a daily classification of synoptic weather patterns, is used. Empirical models of normalized SW irradiance are constructed based on the GWL, relating the synoptic weather patterns to the local radiative climate. In summer, a temporary SW peak in the 1970s and subsequent dimming is linked to variations in the synoptic patterns over Scandinavia, possibly related to a northward shift in the North Atlantic storm track. In spring, a decrease of anticyclonic and increase of cyclonic weather patterns over northern Europe contributes to the dimming from the 1960s to 1990. At many sites, there is also a residual SW irradiance trend not explained by the GWL model: a weak nonsignificant residual dimming from the 1950s or 1960s to around 1990, followed by a statistically significant residual brightening. It is concluded that factors other than the large-scale circulation (e.g., decreasing aerosol emissions) also play an important role in northern Europe.

 Denotes Open Access content.

 Supplemental information related to this paper is available at the Journals Online website: <http://dx.doi.org/10.1175/JCLI-D-15-0476.s1>.

Corresponding author address: Kajsa M. Parding, Norwegian Meteorological Institute, Department of Research and Development, Henrik Mohns plass 1, Oslo 0313, Norway.
E-mail: kajsa.parding@met.no

1. Introduction

Shortwave (SW) irradiance from the sun is the external source of energy on Earth, a fundamental component of the climate system and an increasingly important source of renewable energy in human industrial endeavors (Jacobson and Delucchi 2011). Therefore, it is important



This article is licensed under a [Creative Commons Attribution 4.0 license](https://creativecommons.org/licenses/by/4.0/).

to study changes in SW irradiance on various time scales and their underlying causes.

Observational studies have reported strong decadal-scale trends of SW irradiance, with a widespread decrease of SW irradiance from the 1950s to the 1980s followed by a positive SW irradiance trends in many regions including Europe (Stanhill and Cohen 2001; Liepert 2002; Wild et al. 2005; Russak 2009; Gilgen et al. 2009; Liley 2009; Sanchez-Lorenzo et al. 2015). Decadal SW irradiance trends are commonly referred to as global dimming and brightening, where global refers to “global irradiance,” a term for total (diffuse + direct) hemispheric shortwave irradiance on Earth’s surface (Wild 2012). Although observed SW trends are on the order of several watts per square meter (W m^{-2}) per decade, at many stations the trends are not statistically significant (Chiacchio and Wild 2010; Hinkelman et al. 2009). Nevertheless, there are indications that global dimming from the 1950s to 1980s weakened the hydrological cycle (Liepert et al. 2004; Liepert and Romanou 2005) and influenced plant photosynthesis (Wild 2012; Mercado et al. 2009), reduced the diurnal range of surface temperatures (Wild et al. 2007), and partially masked global warming (Murphy et al. 2009; Wild et al. 2007). Because the observed SW irradiance variability at Earth’s surface is larger than the variability of corresponding measurements at the top of the atmosphere (Fröhlich 2009), changes in solar output are not a likely explanation of dimming and brightening. In this study we will investigate potential causes of dimming and brightening in northern Europe, because clouds are so dominant in this region.

Previous studies have attributed the observed dimming and brightening to changes in clouds and atmospheric aerosols (Liepert 2002; Long et al. 2009; Russak 1990; Ohvri et al. 2009; Streets et al. 2006). Studying the cloud radiative effect, Norris and Wild (2007) found that cloud cover changes contribute to the average pan-European SW irradiance variability but cannot explain all observed dimming and brightening in Europe. They conclude that there is a significant multidecadal direct aerosol radiative effect. In northern Europe, decadal trends of opposite sign in cloud cover and SW irradiance trends, which is expected in periods of cloud-driven dimming or brightening, have been reported in some but not all stations and months (Stjern et al. 2009). On the other hand, cloud cover is not a complete measure of cloud properties. For example, the observed SW dimming in the Tibetan Plateau in the last three decades cannot be explained by changes in the total cloud cover, but Yang et al. (2012) have connected it to an increase in water vapor amount and deep convective clouds. A later study by You et al.

(2013), however, has also reported a significant aerosol radiative effect in the same region.

Qualitative anthropogenic aerosol emission records coincide with the large-scale patterns of global dimming and brightening (Streets et al. 2006). Therefore, long-term aerosol variations are often cited as the main cause of observed dimming and brightening (Wild 2012). Recent modeling studies taking aerosol histories into account indicate that the direct effect of aerosols, scattering and absorbing solar radiation, can account for a large part of the observed dimming and brightening in Europe, while the indirect effect of aerosols on clouds has a smaller effect on SW irradiance (Turnock et al. 2015; Nabat et al. 2014; Folini and Wild 2011; Ruckstuhl and Norris 2009). Natural cloud variations also add to the SW irradiance variability, reducing the dimming or brightening in different periods and regions Folini and Wild (2011). In northern Europe, where aerosol loadings are relatively small compared to other parts of Europe (Turnock et al. 2015), observed dimming and brightening has been connected to both variations in atmospheric aerosol loads and natural cloud variations (Stjern et al. 2009; Parding et al. 2014, 2016).

In this study, we wish to separate the direct and indirect aerosol radiative effects from the influence of natural cloud variations. To do so, we focus on the influence of atmospheric circulation on SW irradiance. It is only recently that the role of atmospheric circulation in global dimming and brightening has become the target of investigation (Sanchez-Lorenzo et al. 2008, 2009; Chiacchio and Wild 2010; Chiacchio et al. 2010, 2011; Chiacchio and Vitolo 2012). In Alaska, Chiacchio et al. (2010) found that cloud changes associated with the Pacific decadal oscillation (PDO) play a major role for SW irradiance variability. Studying solar irradiance and cloud variability at the Iberian Peninsula, Sanchez-Lorenzo et al. (2009) identified a North Atlantic Oscillation (NAO)-like pattern as well as a more local circulation pattern associated with the interannual and decadal variability of cloud cover and sunshine duration. Chiacchio et al. (2011) also established a link between the NAO and sulfate aerosols in Europe, though cause and effect is not clear. In later studies focusing on dimming and brightening in Europe, Chiacchio and Wild (2010) demonstrated that in winter and autumn, the NAO has an important contribution to decadal SW irradiance variability primarily via its influence on low and midlevel clouds. In spring and summer, the SW irradiance variability in northern Europe is connected to the North Sea–Caspian pattern (NCP), an east–west-oriented climate pattern calculated as the geopotential height difference between the North Sea and the northern Caspian Sea (Chiacchio and Vitolo 2012).

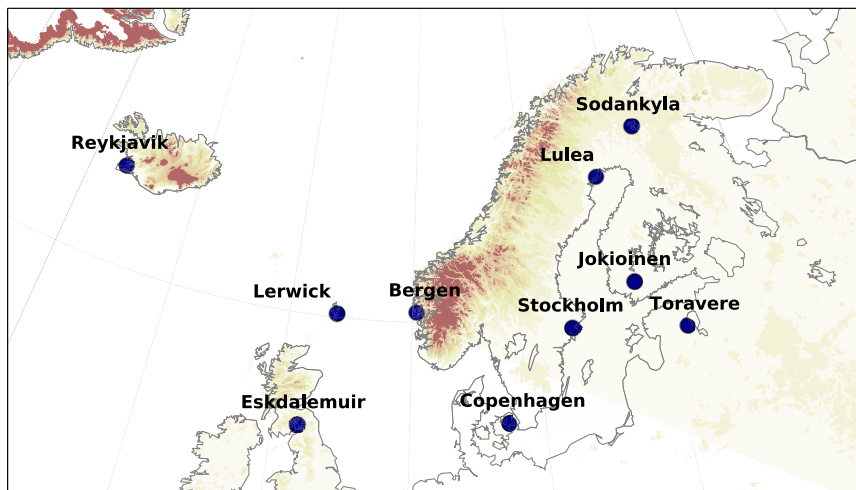


FIG. 1. Map of northern Europe showing the observational stations included in this study (see Table 1).

In this study, compared to previous work, we investigate more broadly the dynamical contribution to dimming and brightening, focusing on atmospheric circulation and its influence on SW irradiance in northern Europe. We focus on spring and summer because of the short day length in northern European winter. As a measure of atmospheric circulation patterns, we use the Grosswetterlagen (GWL) dataset, a daily classification of synoptic weather patterns (Baur et al. 1944; Werner and Gerstengarbe 2010). Compared to climate indices, the GWL dataset has the advantage of providing a temporally more detailed and versatile account of atmospheric circulation, including both NAO- and NCP-like weather patterns. Based on the GWL dataset, we construct empirical linear models of normalized SW irradiance for 10 sites in northern Europe, calibrating the model with daily SW irradiance observations. This method is used in Parding et al. (2016) to investigate the influence of large-scale weather patterns on the cloudiness and shortwave irradiance in Bergen, Norway. The GWL models represent the portion of local SW irradiance variability that is associated with the large-scale atmospheric circulation. The residual of the observed and modeled SW irradiance can be interpreted as the portion of SW irradiance variability that is caused by other factors, such as varying aerosol emissions or small-scale meteorological processes.

2. Data

a. Shortwave irradiance observations

Data from two SW irradiance datasets are used in this study: monthly averaged time series from the Global Energy Balance Archive (GEBA; Gilgen and Ohmura 1999)

and daily averaged observations from the World Radiation Data Centre (WRDC). Although WRDC and GEBA are based on the same surface observations at many locations, the WRDC data are available for a shorter time period (1964–93) than data from the GEBA dataset. For our spatial domain (Europe north of 55°N), we identify 10 stations with no periods of missing WRDC data longer than 2 months and with GEBA data going back to 1965 or longer (Fig. 1, Table 1). The daily averaged observations (WRDC) are used for model calibration as described in section 3a. The longer monthly time series (GEBA) are used for model validation (see Figs. 3–6; Tables 2, 3, and 5).

Gilgen et al. (1998) estimated that the relative random error of measurement for the monthly GEBA SW

TABLE 1. Information about the observational global irradiance data used in this study: monthly time series from the GEBA and daily from the WRDC or obtained via personal communication (Bergen and Toravere). The daily and monthly time series are based on the same observational data but the GEBA dataset tends to cover a longer period of time. The first column (abbr.) is the abbreviation for the station name that we use in this paper.

| Abbr. | Name | Lat | Lon | Years | |
|-------|-------------|---------|---------|-----------|---------|
| | | | | GEBA | WRDC |
| SOD | Sodankyla | 67.37°N | 26.65°E | 1953–2007 | 1964–93 |
| LUL | Lulea | 65.55°N | 22.13°E | 1965–2007 | 1965–93 |
| REY | Reykjavik | 64.13°N | 20.10°W | 1957–2007 | 1964–93 |
| JOK | Jokioinen | 60.82°N | 23.50°E | 1957–2007 | 1964–93 |
| BER | Bergen | 60.39°N | 5.32°E | 1965–2007 | 1965–93 |
| LER | Lerwick | 60.13°N | 0.82°W | 1952–2007 | 1964–93 |
| STO | Stockholm | 59.35°N | 17.95°E | 1922–2007 | 1965–93 |
| TOR | Toravere | 58.27°N | 26.47°E | 1955–2007 | 1964–93 |
| COP | Copenhagen | 55.67°N | 12.30°E | 1965–2002 | 1965–93 |
| ESK | Eskdalemuir | 55.32°N | 2.8°W | 1956–2007 | 1964–93 |

irradiance time series is approximately 5%. SW irradiance observations are subjected to up to five quality tests before they are incorporated into the GEBA archive (Gilgen and Ohmura 1999). Data that have been flagged as erroneous or suspect by one or more of the GEBA quality tests are excluded from this study. The 10 SW irradiance series used in this study have been proved to be homogeneous as reported by Sanchez-Lorenzo et al. (2013). To ensure the quality of the WRDC dataset, we exclude days for which the observed surface SW irradiance is higher than the calculated daily averaged SW irradiance at the top of the atmosphere. To further test the WRDC data quality, we compare monthly averaged WRDC time series to the corresponding GEBA data. For the 10 stations included in this study, the correlation coefficient R between the GEBA and WRDC time series is high ($R > 0.99$) and the bias is low ($< 1 \text{ W m}^{-2}$ for all stations).

To reduce the seasonal and latitudinal variability, the observed downwelling SW irradiance at Earth's surface ($\text{SW}\downarrow_{\text{sfc}}$) is divided by the incoming SW irradiance at the top of the atmosphere ($\text{SW}\downarrow_{\text{TOA}}$). This normalized quantity is referred to as the atmospheric transmittance or Tr , such that $\text{Tr} = \text{SW}\downarrow_{\text{sfc}}/\text{SW}\downarrow_{\text{TOA}}$. The value of $\text{SW}\downarrow_{\text{TOA}}$ is calculated based on time and location as described in Iqbal (1983, 59–69) with a solar constant of 1361 W m^{-2} (Kopp and Lean 2011). The daily (WRDC) and monthly (GEBA) averaged observed SW irradiance values are normalized using daily and monthly averages of a calculated 5-min $\text{SW}\downarrow_{\text{TOA}}$ time series. Theoretically possible values of Tr range from 0 (opaque atmosphere; all SW irradiance has been scattered back to space or absorbed in the atmosphere) to 1 (transparent atmosphere; all incoming top-of-atmosphere SW irradiance has been transmitted to the surface of Earth).

Seasonally averaged time series of observed Tr for spring (MAM) and summer (JJA) are calculated from monthly averaged observational values. If one of the three monthly values is missing in a season, the missing value is replaced with a climatological monthly value. If more than one monthly value is missing, the seasonal average for the year is considered missing. The climatological value is calculated based on the 15 years before and after the missing value. The sliding climatology is preferred over using a standard period climatology because in time series with long-term trends, values from a different period may not be representative of the climatology when the missing value occurs.

b. Grosswetterlagen

As a measure of synoptic meteorological patterns, we use the Grosswetterlagen, a subjective weather classification first developed by Baur et al. (1944) in the 1940s

and revised by Hess and Brezkowsky in 1950/51 (Werner and Gerstengarbe 2010). The classification is done manually and has been carried out by the German weather service for data from 1881 to the present day, until 1938 based on sea level pressure (SLP) observations alone and since 1939 with the additional information of 500-hPa geopotential height maps (Werner and Gerstengarbe 2010). The GWL dataset catalogues the occurrence of 29 common weather patterns, which we refer to as GWL 1–29. Descriptions of the GWL weather patterns and the abbreviated German names that they are often referred to by are shown in Table S1 of the supplementary material. The weather patterns are characterized by the position of cyclonic and anticyclonic weather systems and the surface flow over the North Atlantic and Europe, with a focus on central Europe. Each day is prescribed exactly one GWL pattern and that GWL must persist unchanged for a minimum of 3 days. Days that do not fit any of GWL 1–29 or occur less than 3 days in a row have been prescribed GWL 30 = unknown (very rare; $< 1\%$ of all days are prescribed GWL 30). This is not to say that the synoptic weather situation is constant on scales shorter than 3 days, but that GWL represents a general structure that changes only slowly. Figure 2 shows the average SLP patterns of 14 GWL weather patterns for 1979–2013 that are identified as particularly important to SW irradiance variability in northern Europe (see section 5). The SLP maps are calculated based on daily NCEP–DOE Reanalysis 2 (Kanamitsu et al. 2002) data provided by the NOAA/OAR/ESRL Physical Sciences Division (PSD) (Boulder, Colorado; <http://www.esrl.noaa.gov/psd/>).

3. Methods

a. GWL models of atmospheric transmittance

For each site listed in Table 1 and shown in Fig. 1, an empirical linear model of Tr is constructed from the frequencies of GWL 1–29 and the daily observed SW irradiance, separately for each station and season. The GWL models represent the relationship between the large-scale meteorological situation and the local variations of SW irradiance (Parding et al. 2016). In this study, we focus on the spring (MAM) and summer (JJA) seasons, because there is little SW irradiance during the winter half-year at the high-latitude sites investigated here. The linear GWL models are calculated as follows:

$$\text{Tr}_{\text{model}}(y) = c_0 + \sum_{i=1}^{29} c_i f_i(y), \quad (1)$$

where $c_0 = \widetilde{\text{Tr}}(d)$ and $c_i = \widetilde{\text{Tr}}(d_i) - c_0$ with $d_i \in d[\text{GWL } i]$, $f_i(y)$ is the seasonally averaged frequency of the weather

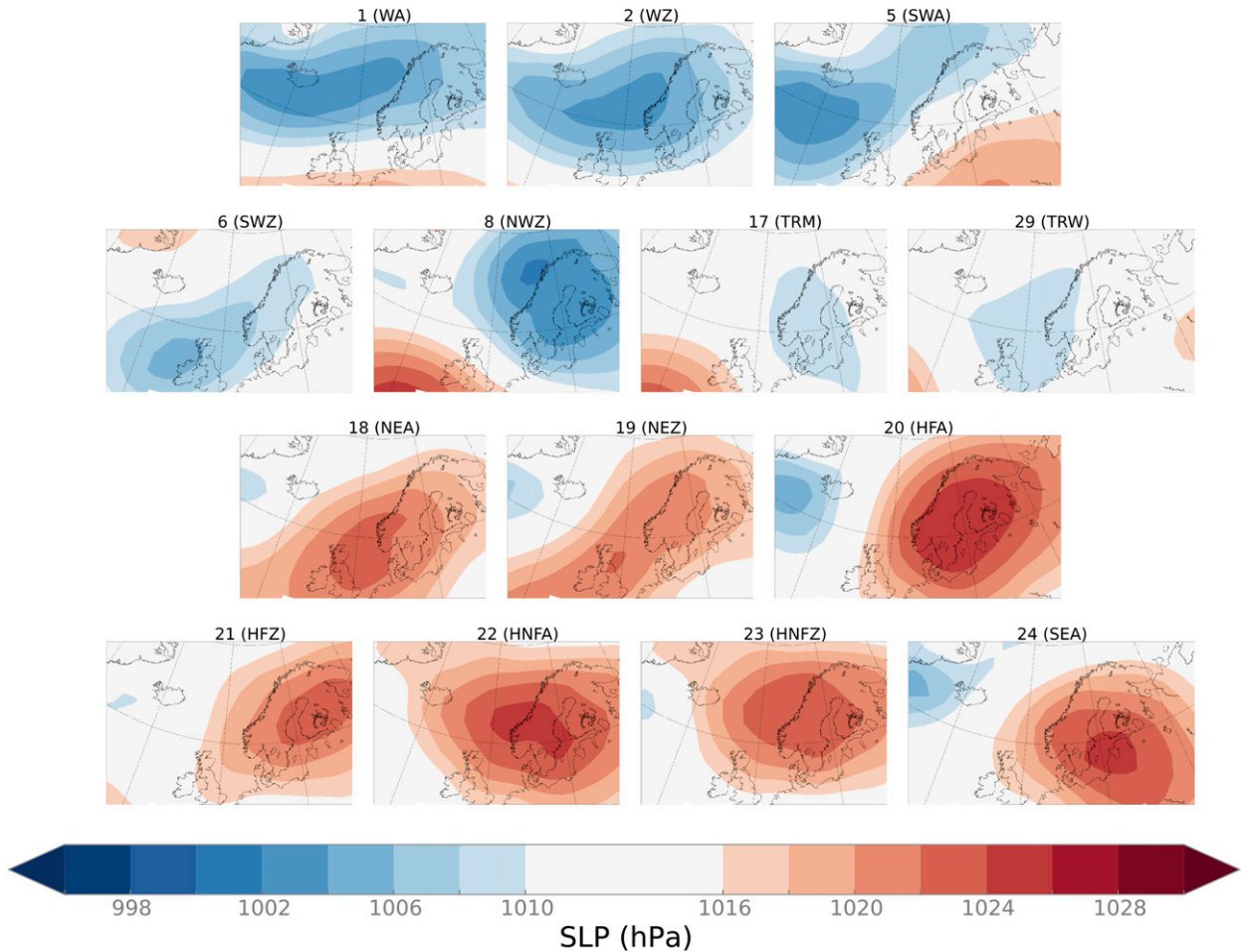


FIG. 2. Sea level pressure (SLP) maps for 14 Grosswetterlagen weather patterns (see section 2b) that are identified as particularly important to SW irradiance in northern Europe in section 5c.

pattern GWL i ($i = 1-29$) for years y ($y = 1881-2013$), and $\text{Tr}(d)$ and $\text{Tr}(d_i)$ are the daily observed atmospheric transmittance time series for all days and days that have been identified as GWL i , respectively. The coefficients c_i are calculated as the difference between the median value of $\text{Tr}(d_i)$ and $\text{Tr}(d)$. We use the median value rather than the mean to estimate the anomalies because the median is less affected by outliers. Daily SW irradiance data from 1964 to 1993 are used for model calibration (i.e., to calculate the coefficients c_0 and c_i).

A positive coefficient ($c_i > 0$) indicates that the weather pattern GWL i is associated with positive anomalies of atmospheric transmittance (i.e., more sunny conditions than average). Negative coefficients show that the weather pattern is associated with less atmospheric transmittance than usual and implies the presence of clouds. A coefficient close to zero indicates that there is little connection between the SW irradiance and weather pattern GWL i , because the average transmittance for

GWL i does not deviate much from the average transmittance for all days. In general, if there is no connection between the surface irradiance and synoptic weather patterns, then all coefficients $c_1 \approx c_2 \approx c_3 \approx \dots \approx c_{29} \approx 0$, resulting in a model with very little variability. As seen in section 4, this is not the case at most sites.

Given enough data for model calibration, the GWL model represents the portion of SW variability that is related to large-scale atmospheric circulation. However, for seldom-occurring weather patterns, the coefficients have to be calculated based on few data points which may not be representative of the relationship between the weather patterns and local surface solar conditions. In the small number of cases where fewer than 10 data points are available to estimate a coefficient, the coefficient is therefore set to zero. For the calibration period considered here (1964–93), the only coefficients set to zero were GWL 27 for the spring season and GWL 25, 26, and 27 for summer.

b. Jackknife sensitivity test

To estimate the sensitivity of the models to the calibration period, we apply a jackknife resampling method. The jackknife test provides a measure of how robust the models are with respect to the data used for model calibration—that is, whether there is a stationary statistical relationship between the large-scale weather patterns (GWL) and the local atmospheric transmittance.

The jackknife procedure is done by dividing the daily averaged atmospheric transmittance time series (WRDC data, 1964–93) into five parts and five times recalculating the 29 model coefficients [c_i in Eq. (1), where i represents one of the 29 GWL types] while leaving one of the parts out. The standard deviation σ_J of the model coefficient c_i is estimated based on the jackknife distribution $\{\hat{c}_{i(1)}, \hat{c}_{i(2)}, \hat{c}_{i(3)}, \hat{c}_{i(4)}, \hat{c}_{i(5)}\}$ [see Eq. (2)]:

$$\sigma_J = \sqrt{\frac{1}{5} \sum_{j=1}^5 [\hat{c}_{i(j)} - \bar{c}_i]^2}, \quad (2)$$

where $\bar{c}_i = (1/5) \sum_{j=1}^5 \hat{c}_{i(j)}$.

The standard deviation of the model reconstruction $[\text{Tr}_{\text{model}}(y)]$ is estimated based on the standard deviations of the coefficients.

c. Statistical measures of goodness of fit

To assess the performance of the GWL models with respect to observed atmospheric transmittance, we calculate the following statistical measures: the bias [Eq. (3)], the root-mean-square deviation [RMSD; Eq. (4)], and the Pearson's product moment correlation coefficient [R , Eq. (5)]:

$$\text{bias} = \frac{1}{N} \sum_{j=1}^N [\text{Tr}(y_j) - \text{Tr}_{\text{model}}(y_j)], \quad (3)$$

$$\text{RMSD} = \sqrt{\frac{1}{N} \sum_{j=1}^N [\text{Tr}(y_j) - \text{Tr}_{\text{model}}(y_j)]^2}, \quad \text{and} \quad (4)$$

$$R = \frac{\sum_{j=1}^N [\text{Tr}(y_j) - \bar{\text{Tr}}][\text{Tr}_{\text{model}}(y_j) - \bar{\text{Tr}}_{\text{model}}]}{\sqrt{\sum_{j=1}^N [\text{Tr}(y_j) - \bar{\text{Tr}}]^2} \sqrt{\sum_{j=1}^N [\text{Tr}_{\text{model}}(y_j) - \bar{\text{Tr}}_{\text{model}}]^2}}, \quad (5)$$

where

$$\bar{\text{Tr}} = \frac{1}{N} \sum_{j=1}^N \text{Tr}(y_j) \quad \text{and} \quad \bar{\text{Tr}}_{\text{model}} = \frac{1}{N} \sum_{j=1}^N \text{Tr}_{\text{model}}(y_j).$$

In the equations above, Tr and Tr_{model} represent the seasonally averaged observed and model-simulated atmospheric transmittance for the years y_j . The length N

of the seasonal mean time series varies from site to site depending on the length of the observational time series (see Table 1).

The bias has been defined here so that a positive value indicates that the observed values are, on average, higher than the corresponding modeled values. The RMSD is a measure of the magnitude of the deviations of modeled from observed values. The term R measures the proportional changes in two time series and goes from -1 (perfect anticorrelation) via 0 (no correlation) to 1 (perfect correlation). The square of the correlation coefficient, R^2 , is an estimate of the explained variance. The statistical significance of the correlation between modeled and observed Tr is estimated by a permutation test as described in section 3d. When calculating the correlation between Tr at different stations (Tables 3–5), the statistical significance of R is estimated by a two-tailed Student's t test.

The statistical comparison of observed and model simulated time series is calculated based on the full period of available observational data of each location and season, which ranges from 38 to 86 years depending on the site (see length of the GEBA time series in Table 1).

d. Permutation test

A permutation test is done to estimate the statistical significance of the correlation coefficient R of modeled and observed Tr . The first step of the permutation test is to randomly rearrange the order of the GWL time series so that they no longer represent real occurrences of synoptic weather patterns, but rather a collection of 29 random binary time series with the same distribution as the GWL dataset. To maintain the properties of the GWL dataset we rearrange the time series of GWL 1–29 in the same order and in blocks of five days, which is the average persistence of the GWL weather patterns. Then models of transmittance are fitted as previously described based on the 29 randomized time series. Finally, an R value is calculated based on the randomized Tr model and the Tr observations. The procedure is repeated 5000 times, resulting in a perturbation distribution that can be used to estimate the probability p of randomly obtaining a model that produces a value as high as R .

e. Confidence intervals of observed, modeled, and residual Tr

The standard deviations σ of the observations are calculated assuming a 5% relative measurement uncertainty of the monthly SW irradiance observations (Gilgen et al. 1998). When normalizing the SW irradiance and calculating the seasonal averages (section 2a), the total uncertainty is calculated using the

TABLE 2. Statistical measures comparing model simulations and observations of atmospheric transmittance for the summer (JJA) and spring (MAM) seasons. The atmospheric transmittance, Tr , is a normalized version of the surface SW irradiance (surface SW irradiance/top-of-atmosphere SW irradiance). The terms $\overline{\text{Tr}}_{\text{obs}}$ and $\overline{\text{Tr}}_{\text{model}}$ are the seasonal mean values of observed and modeled Tr (see section 2a). The mean values are reported with a confidence interval of two standard deviations ($\pm 2\sigma$). The other statistical estimators are the bias, RMSD, and Pearson's correlation coefficient R , defined in section 3c. The statistical significance of R is estimated by a permutation test (section 3d) and results are presented as p , the probability of obtaining a result by random. Results shown in this table are calculated based on the total period of available monthly SW irradiance observations which is not the same for all stations (see Table 1). The bias and RMSD have the same scale as the atmospheric transmittance whereas R is a unitless measure of the model goodness of fit ranging from -1.0 (perfect anticorrelation) via 0 (no correlation) to $+1.0$ (perfect correlation).

| Station | Season | $\overline{\text{Tr}}_{\text{obs}}$ | $\overline{\text{Tr}}_{\text{model}}$ | Bias | RMSD | R | p |
|---------|--------|-------------------------------------|---------------------------------------|-----------|------|------|--------|
| SOD | MAM | 0.50 ± 0.08 | 0.50 ± 0.04 | -0.0004 | 0.03 | 0.52 | 0.004 |
| LUL | MAM | 0.50 ± 0.07 | 0.51 ± 0.04 | -0.01 | 0.03 | 0.65 | <0.001 |
| REY | MAM | 0.43 ± 0.08 | 0.41 ± 0.04 | $+0.02$ | 0.04 | 0.43 | 0.012 |
| JOK | MAM | 0.48 ± 0.09 | 0.47 ± 0.06 | $+0.009$ | 0.04 | 0.51 | 0.002 |
| BER | MAM | 0.39 ± 0.08 | 0.38 ± 0.07 | $+0.01$ | 0.03 | 0.64 | <0.001 |
| LER | MAM | 0.40 ± 0.06 | 0.38 ± 0.03 | $+0.01$ | 0.03 | 0.31 | 0.09 |
| STO | MAM | 0.48 ± 0.09 | 0.49 ± 0.06 | -0.01 | 0.05 | 0.18 | 0.13 |
| TOR | MAM | 0.47 ± 0.08 | 0.47 ± 0.05 | -0.003 | 0.04 | 0.49 | <0.001 |
| ESK | MAM | 0.37 ± 0.06 | 0.36 ± 0.03 | $+0.01$ | 0.03 | 0.47 | <0.001 |
| COP | MAM | 0.45 ± 0.08 | 0.46 ± 0.05 | -0.01 | 0.04 | 0.59 | <0.001 |
| SOD | JJA | 0.45 ± 0.09 | 0.44 ± 0.04 | $+0.01$ | 0.04 | 0.58 | <0.001 |
| LUL | JJA | 0.49 ± 0.07 | 0.50 ± 0.04 | -0.01 | 0.03 | 0.63 | <0.001 |
| REY | JJA | 0.41 ± 0.08 | 0.38 ± 0.04 | $+0.03$ | 0.04 | 0.70 | <0.001 |
| JOK | JJA | 0.48 ± 0.08 | 0.48 ± 0.05 | $+0.002$ | 0.03 | 0.65 | <0.001 |
| BER | JJA | 0.40 ± 0.08 | 0.39 ± 0.07 | $+0.002$ | 0.03 | 0.64 | <0.001 |
| LER | JJA | 0.39 ± 0.06 | 0.38 ± 0.02 | $+0.01$ | 0.03 | 0.52 | <0.001 |
| STO | JJA | 0.49 ± 0.11 | 0.51 ± 0.05 | -0.004 | 0.05 | 0.47 | <0.001 |
| TOR | JJA | 0.48 ± 0.08 | 0.50 ± 0.04 | -0.01 | 0.03 | 0.59 | <0.001 |
| ESK | JJA | 0.38 ± 0.07 | 0.38 ± 0.04 | $+0.003$ | 0.02 | 0.76 | <0.001 |
| COP | JJA | 0.48 ± 0.09 | 0.49 ± 0.05 | -0.008 | 0.04 | 0.66 | <0.001 |

general law of error propagation (Taylor 1997); for example, for the summer season average $\sigma_{\text{summer}} = (1/3)\sqrt{\sigma_{\text{june}}^2 + \sigma_{\text{july}}^2 + \sigma_{\text{august}}^2}$. For the GWL models, is estimated by jackknife method as described in section 3b. The uncertainty of the residual Tr is estimated from observed and modeled uncertainties as $\sigma_{\text{residual}} = \sqrt{\sigma_{\text{obs}}^2 + \sigma_{\text{model}}^2}$.

4. Results

a. Evaluation of GWL model performance

Based on the correlation between modeled and observed transmittance for the 10 stations, the GWL models explain 22%–58% of the variance of seasonally averaged observed transmittance in summer but only 3%–42% in spring (see Table 2). The deviation of model simulations from observations as measured by the RMSD is between 0.03 and 0.05 (5%–10% of the average observed Tr) depending on season and site (Table 2). The largest RMSD values are found in Stockholm and Reykjavik. The mean bias deviation of the GWL models tend to be small, with the exception of Reykjavik, which has a bias of $+0.03$ (7%) for summer.

Figures 3 and 4 show the time series of observed and modeled transmittance for the individual stations in the

spring and summer, respectively. The highest correlation between modeled and observed transmittance is obtained for Eskdalemuir in the summer season ($R = 0.76$). The visual comparison confirms that the model represent the observed transmittance at the station well in summer (Fig. 4). On the other hand, the second highest correlation is found at Reykjavik ($R = 0.70$), also in summer, even though visual inspection shows that the modeled and observed Tr do not agree well in terms of the range of the transmittance and the GWL model tends to estimate lower values than observed. This example demonstrates how the insensitivity of Pearson's correlation coefficient, R , to the scale of the variations and systematic differences can be a weakness when it is used as a measure of model performance. Low correlation coefficients, as found in Stockholm and Lerwick, can be interpreted as an indication that the GWL models do not agree well with observed transmittance. The mediocre correlations at most of the other sites are not as informative without considering the visual inspection or other statistical measures of model performance.

Nevertheless, permutation tests show that the correlation between observed and modeled Tr is statistically significant at the 95% level ($p < 0.05$) for all stations in

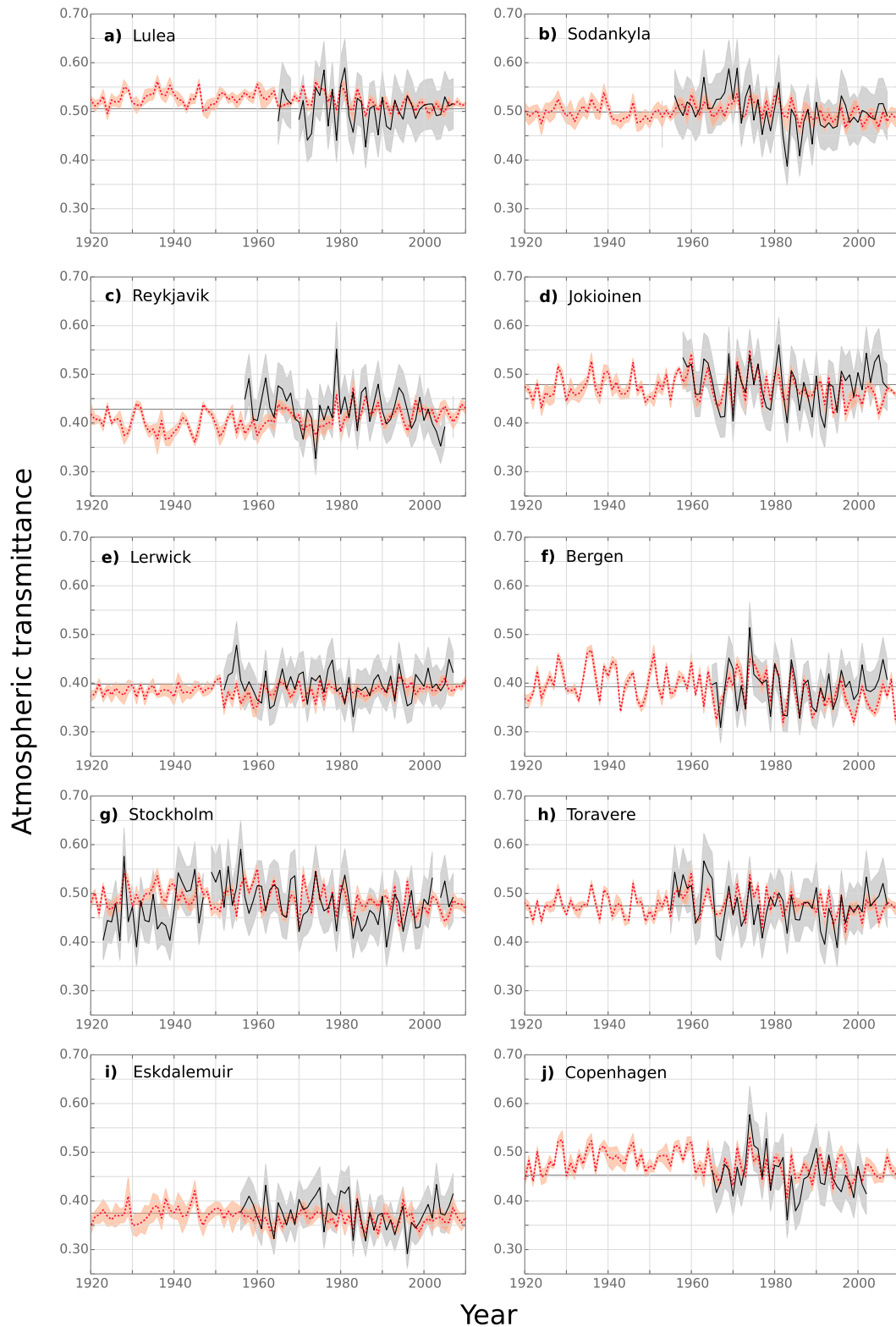


FIG. 3. Seasonal mean time series of the modeled (red dotted line) and observed (black solid line) atmospheric transmittance for the spring season (MAM). The atmospheric transmittance models are constructed based on the Grosswetterlagen dataset and global irradiance measurements as described in Eq. (1). Confidence intervals ($\pm 2\sigma$) of the modeled and observed transmittance are calculated as described in section 3e and are shown here as shaded areas.

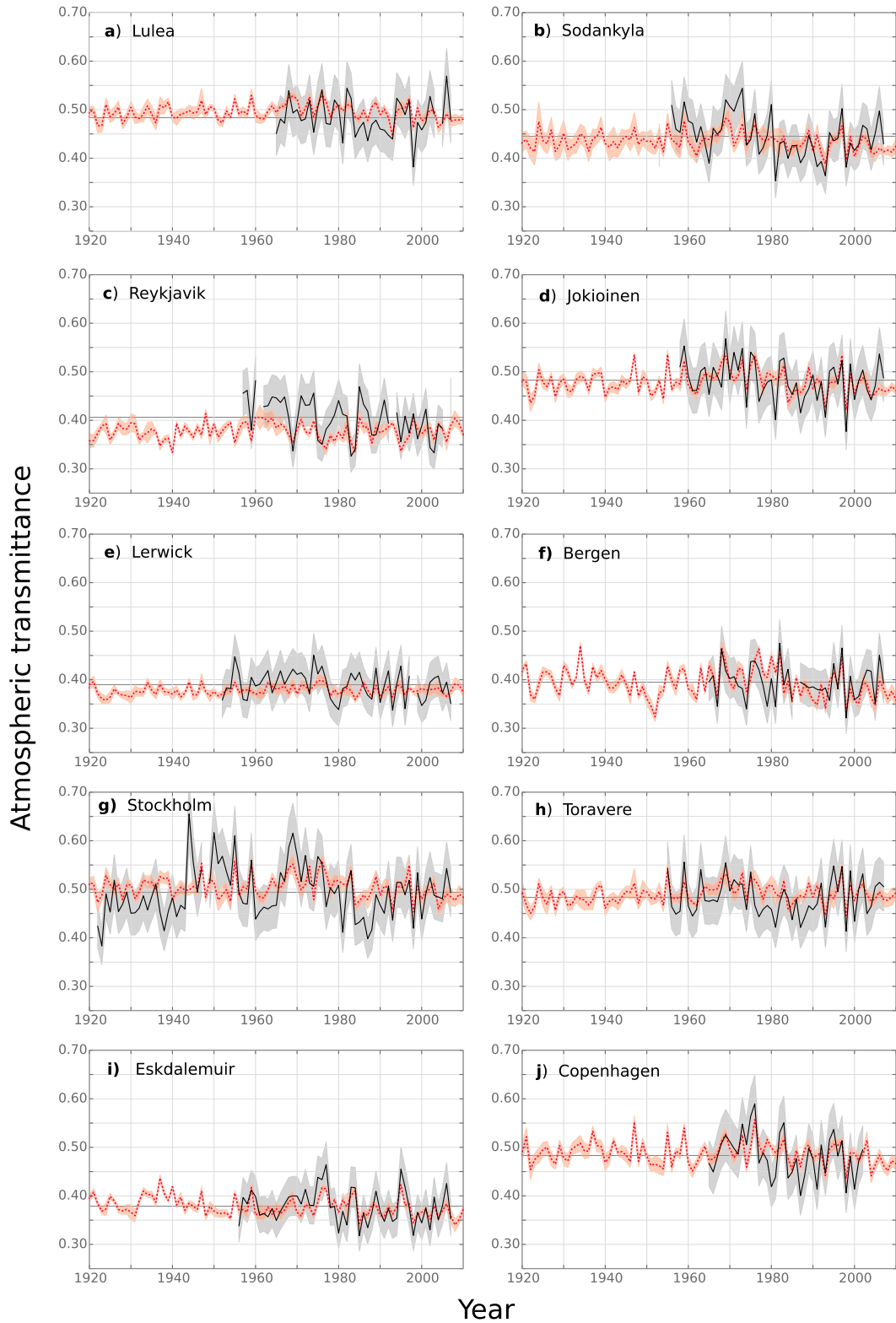


FIG. 4. As in Fig. 3, but for the summer season (JJA).

summer and for a majority of stations in spring. This means that (with the exception of Stockholm and Lerwick in spring) the observed Tr values agree better with Tr reconstructions based on the GWL dataset than expected from models based on randomized data. The result of the permutation tests indicates that there is a significant link between large scale weather patterns and the local atmospheric transmittance variability that is represented by the GWL models.

Visual inspection of Figs. 3 and 4 indicates that although GWL models cannot explain all year-to-year variability of observed Tr, there are stations and periods where modeled and observed Tr are in agreement. Jokioinen stands out as the station where the GWL model best represents observed Tr. In summer, modeled Tr in Jokioinen is within the confidence interval (CI) of the observed Tr in almost all years (Fig. 4d). In spring, the modeled and observed Tr follow each other closely until the mid-1990s after which there is an observed Tr increase that is not represented by the GWL model (Fig. 3d). In Bergen, agreement between observed and modeled Tr is good until the late 1990s, as reported in a previous study by Parding et al. (2016) (Figs. 3f and 4f). In Eskdalemuir, the GWL model successfully reproduces the observed Tr in summer but the spring GWL model does not perform as well (Figs. 3i and 4i).

In Lulea, Sodankyla, Reykjavik, Stockholm, Toravere, and Copenhagen the results are more difficult to interpret (Figs. 3a–c, 3g–j, 4a–c, and 4g–j). The visual comparison shows large differences between modeled and observed Tr. The GWL models have a smaller range than the observed Tr and rarely reproduce the highest observed Tr peaks. There are, however, periods when the GWL models follow the observed Tr variability. For example, the summer GWL models represent observed Tr very well in the period 1991–2004 at most stations (Sodankyla, Jokioinen, Bergen, Stockholm, Toravere, Eskdalemuir, and Copenhagen).

In Lerwick (Figs. 3e and 4e), the modeled Tr time series is almost flat, a sign of small model coefficients and little connection between the GWL and observed Tr (see discussion at the end of section 3a).

Assuming that the GWL models represent the large-scale circulation portion of SW irradiance variability, the residual of observed and modeled transmittance can be interpreted as the portion of transmittance that is associated with other factors (e.g., local meteorological processes, such as water vapor changes or convective cloud formation, and varying atmospheric aerosol loads). Judging from the residual Tr time series in Figs. 5 and 6, the weather-pattern-independent transmittance variability is the strongest in Stockholm and Sodankyla. In Lerwick, although the GWL model

is a poor representation of observed transmittance variability, the residual is nevertheless small and relatively stable over time (Figs. 5e and 6e) because the observed Tr has relatively small variability and no long-term trend (Figs. 3e and 4e).

For the empirical GWL models to adequately represent the effect of large-scale circulation on local SW irradiance, the relationship between weather patterns and local SW irradiance must be robust (i.e., statistically stationary). The robustness of the empirical GWL models is evaluated based on confidence intervals obtained by jackknife method as described in section 3b. The CI of the modeled Tr, shown as red shaded areas in Figs. 3 and 4, are small compared to the CI of observed Tr (gray shaded areas, same figures). The relatively narrow intervals indicate that the relationship between the GWL weather patterns and locally observed SW irradiance is robust.

b. Spatial correlation of observed, modeled, and residual atmospheric transmittance

Because the GWL models are based on observations of large-scale weather patterns, the modeled transmittance is expected to exhibit a spatial homogeneity. Not surprisingly, the correlation between transmittance time series at different stations is higher for GWL models than for observations (cf. Tables 3 and 4). For widely separated sites such as Copenhagen and Sodankyla, the correlation between observed Tr time series tends to be small and nonsignificant while the GWL models have a higher and often statistically significant correlation even between distant sites. For the residuals (observed minus modeled transmittance), the spatial correlation is lower and statistically significant only in the comparison of neighboring stations (Table 5). Interestingly, the GWL model for Stockholm, which is in poor agreement with observed atmospheric transmittance, is highly correlated with the model for Jokioinen, its closest neighboring station. Based on visual and statistical estimates, the GWL model for Jokioinen represents the observed transmittance reasonably well. The similarity of the GWL models suggest that the modeled Tr represent a transmittance variability that is mutual for the two stations, which appears to be dominant in Jokioinen but only represents a minor portion of the observed Tr variability in Stockholm. An anticorrelation between Tr in Reykjavik and other stations in northern Europe is found, stronger in modeled than observed Tr. In Lerwick, the observed, modeled, and residual transmittance is weakly correlated (or anticorrelated) with the transmittance at other stations.

The more spatially homogeneous character of the GWL models, which isolate the circulation effects on

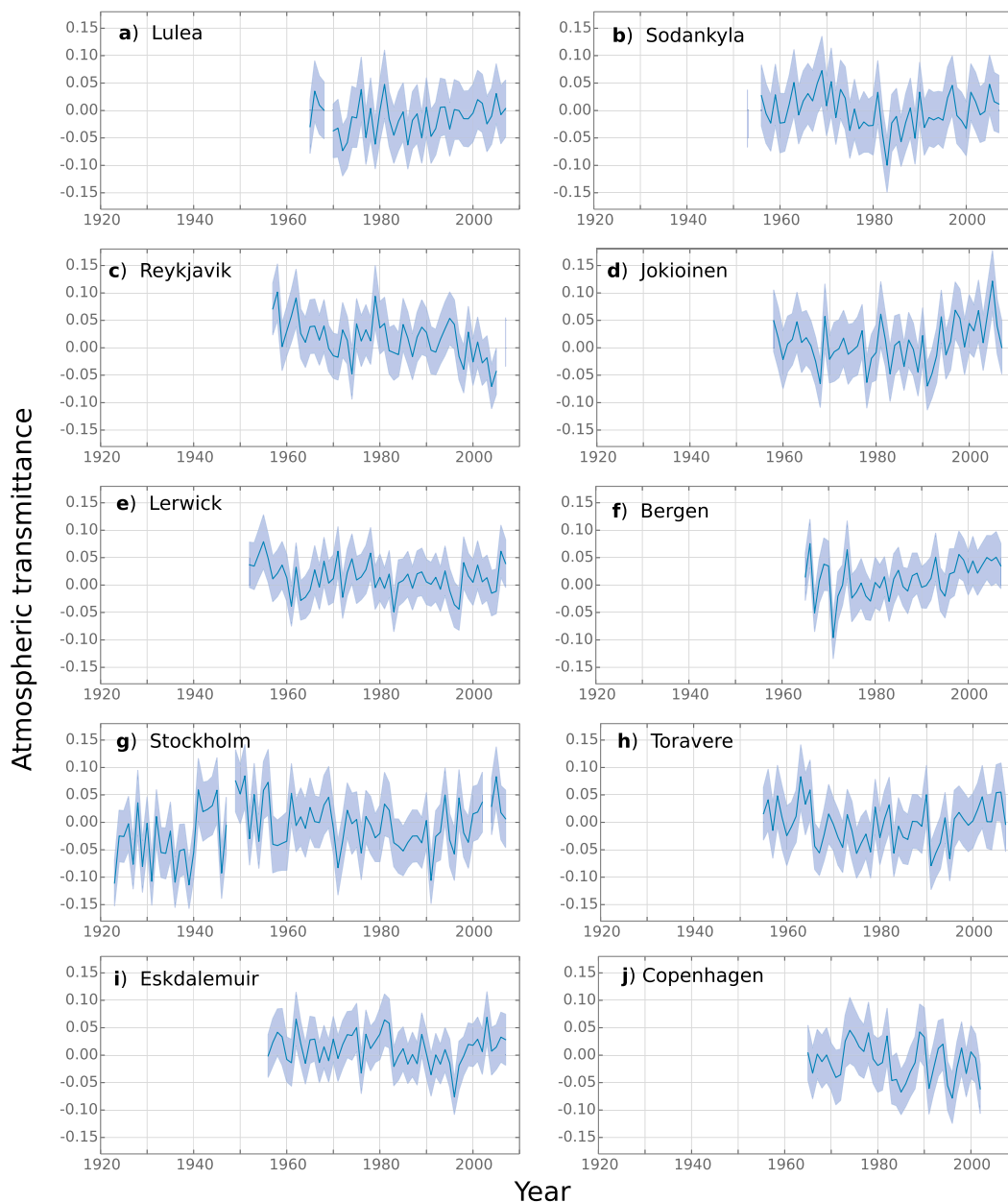


FIG. 5. Seasonal mean time series of the residual (observed – modeled) atmospheric transmittance for the spring season (MAM) based on the observational time series and GWL models presented in Fig. 3. Confidence intervals ($\pm 2\sigma$) of the residual transmittance are calculated as described in section 3e and are shown here as shaded areas.

SW irradiance, in comparison with observed and residual Tr, which are modulated by other influences, is also obvious from Fig. 7, showing regionally averaged Tr time series. The regional average is calculated based on the northern European sites in Fig. 1 except for Lerwick and Reykjavik, which are excluded because of the low or negative correlation with Tr at other sites. The regional GWL model is calculated as the average of the eight individual GWL models.

Regional averages of observed and residual Tr are calculated only for the period 1956–2007 when SW irradiance observations from three or more stations are available. For the GWL models (Figs. 7c,d), the Tr values of individual stations (blue lines) fall close to the regional average (black line). The observed and residual Tr time series (Figs. 7a,b,e,f) have a larger spread and individual stations deviate more from the regional average.

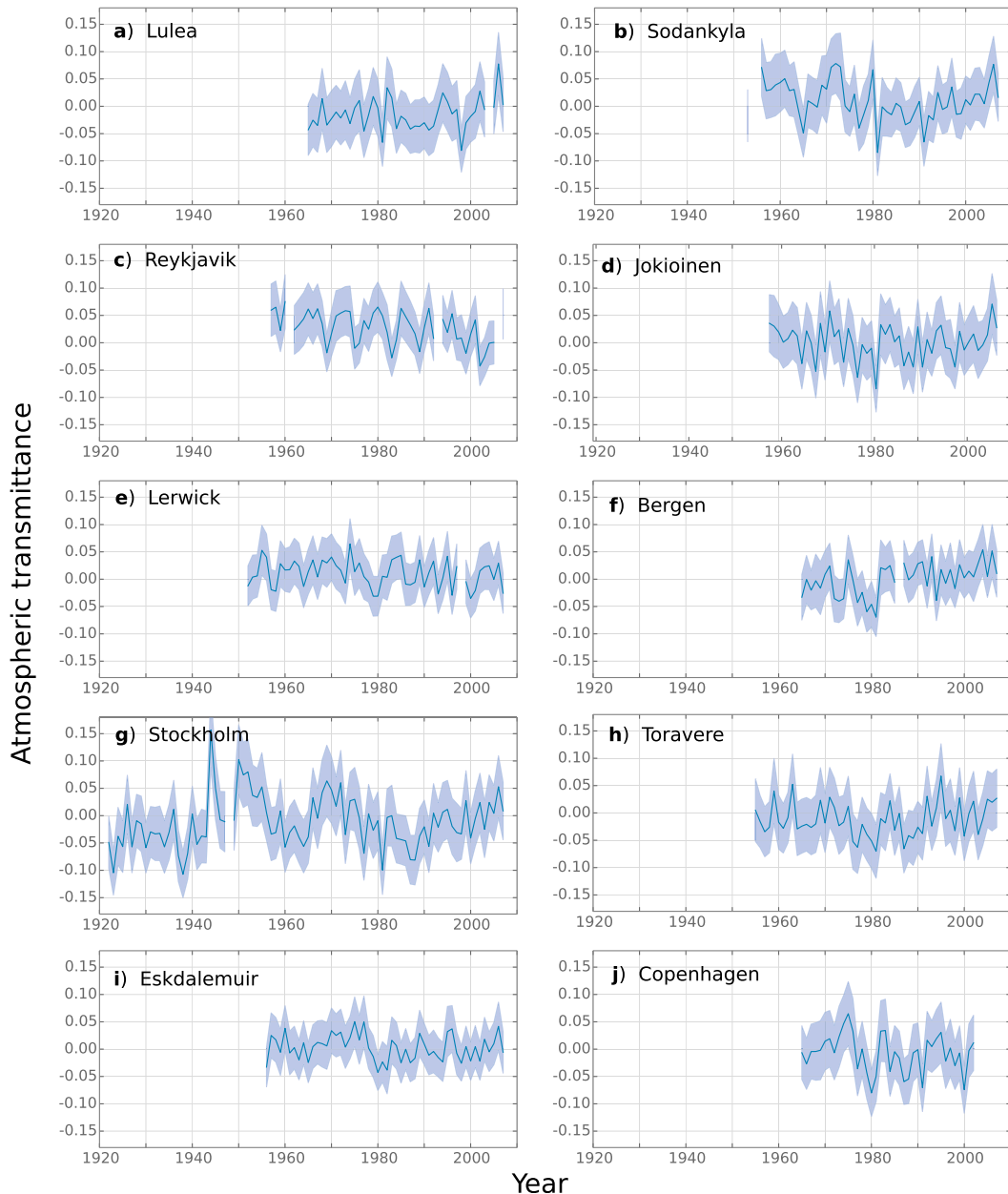


FIG. 6. As in Fig. 5, but for the summer season (JJA) based on the observational time series and GWL models presented in Fig. 4.

c. Decadal variability of observed, modeled, and residual atmospheric transmittance

Estimates of trends in the regionally averaged (not including Lerwick and Reykjavik) observed, modeled, and residual transmittance time series are displayed in Table 6. The trends are estimated by first-order linear regression. The statistical significance of the trends is evaluated by the nonparametric Mann–Kendall (MK) test (Kendall 1962). We use the 95%

level as a criterion for a statistically significant trend but also report the p value (the probability with which the null hypothesis of no trend can be rejected) in Table 6. The periods considered for trend analysis are selected based on the minimum and maximum years of the smoothed observed transmittance time series in Fig. 7. In spring, there is a transmittance minimum in 1989. In summer, the transmittance reaches a maximum in 1972 and a minimum in 1986. Therefore, trend estimates are calculated for 1956–89 and 1989–2007

TABLE 3. Correlation between observations of atmospheric transmittance at different stations. The lower left half of the table represents the summer season (JJA) and the upper right half represents the spring season (MAM). Boldface font denotes correlation coefficients that are statistically significant at the 95% level ($p < 0.05$). The statistical significance is estimated using a two-tailed Student's t test.

| Station | SOD | LUL | REY | JOK | BER | LER | STO | TOR | ESK | COP |
|---------|-------------|-------------|-------|-------------|-------------|-------|-------------|-------------|-------|-------------|
| SOD | | 0.67 | -0.35 | 0.53 | 0.45 | 0.02 | 0.48 | 0.47 | 0.16 | 0.40 |
| LUL | 0.67 | | -0.31 | 0.56 | 0.50 | 0.02 | 0.54 | 0.32 | 0.15 | 0.46 |
| REY | -0.03 | -0.29 | | -0.41 | -0.45 | 0.01 | -0.32 | -0.18 | -0.09 | -0.44 |
| JOK | 0.74 | 0.74 | -0.21 | | 0.47 | -0.25 | 0.63 | 0.73 | 0.11 | 0.35 |
| BER | 0.34 | 0.61 | -0.42 | 0.51 | | 0.09 | 0.41 | 0.37 | 0.23 | 0.36 |
| LER | 0.24 | 0.18 | -0.23 | 0.24 | 0.29 | | 0.01 | -0.16 | 0.45 | 0.28 |
| STO | 0.64 | 0.67 | -0.33 | 0.71 | 0.45 | 0.40 | | 0.55 | 0.21 | 0.61 |
| TOR | 0.53 | 0.55 | -0.32 | 0.79 | 0.43 | 0.39 | 0.72 | | 0.08 | 0.36 |
| ESK | 0.25 | 0.37 | -0.40 | 0.41 | 0.39 | 0.32 | 0.44 | 0.37 | | 0.44 |
| COP | 0.27 | 0.46 | -0.31 | 0.46 | 0.21 | 0.48 | 0.56 | 0.52 | 0.44 | |

in spring and 1956–72, 1972–86, and 1986–2007 in summer.

In spring, the regionally averaged observed Tr decreased by $3.1\% \text{ decade}^{-1}$ during 1956–89, which corresponds to a trend of approximately $-4 \text{ W m}^{-2} \text{ decade}^{-1}$ (Fig. 7a, Table 6). After a trend reversal, the observed Tr increased by $5.6\% \text{ decade}^{-1}$ in 1989–2007, in terms of SW irradiance approximately $+8 \text{ W m}^{-2} \text{ decade}^{-1}$. Both the negative Tr trend and following positive Tr trend, which can be described as a dimming period followed by a brightening, are statistically significant. The regionally averaged GWL model explains almost half of the observed dimming 1956–89 ($-1.4\% \text{ decade}^{-1} \approx -2 \text{ W m}^{-2} \text{ decade}^{-1}$) (Fig. 7c, Table 6). During the observed brightening period after 1989, the modeled Tr did not increase but instead remained relatively stable throughout the 1990s and 2000s. For this reason, there is a statistically significant decrease in modeled Tr but not in the observations or residual Tr over the extended period of 1956–2007. The residual Tr in spring is characterized by a dimming, approximately half as strong as the observed dimming ($-1.8\% \text{ decade}^{-1} \approx -2.5 \text{ W m}^{-2} \text{ decade}^{-1}$), followed by a more pronounced

brightening ($+6.1\% \text{ decade}^{-1} \approx +8 \text{ W m}^{-2} \text{ decade}^{-1}$) (Fig. 7e). Both the residual dimming and brightening over the shorter intervals are statistically significant.

In summer, there is no significant long-term change in observed, modeled or residual Tr from 1956 to 2007 (not shown), but strong changes occur on shorter time scales. During 1956–72, the observed Tr increased by $4.3\% \text{ decade}^{-1}$ ($\approx +8 \text{ W m}^{-2} \text{ decade}^{-1}$), then for the short period 1972–86 declined by $8.2\% \text{ decade}^{-1}$ ($\approx -15 \text{ W m}^{-2} \text{ decade}^{-1}$), and finally in 1986–2007 increased by $4.0\% \text{ decade}^{-1}$ ($\approx +8 \text{ W m}^{-2} \text{ decade}^{-1}$) (Fig. 7b, Table 6). The regional average GWL model explains over 60% of the observed Tr trends directly preceding and following the observed transmittance peak in 1972 (Fig. 7d, Table 6). Neither the modeled nor the observed Tr changes during 1956–72 and 1972–86 are statistically significant at the 95% level, but the modeled trends are significant at the 90% level. In summer, the modeled Tr levels out in the late 1990s as the observed Tr starts to increase again. The residual Tr in summer is, as in spring, characterized by a weak transmittance decline from the 1950s to the late 1980s, followed by a more pronounced increase (Fig. 7f). The

TABLE 4. Correlation between model simulations of atmospheric transmittance at different stations. The lower left half of the table represents the summer season (JJA) and the upper right half represents the spring season (MAM). Boldface font denotes correlation coefficients that are statistically significant at the 95% level ($p < 0.05$). The statistical significance is estimated using a two-tailed Student's t test.

| Station | SOD | LUL | REY | JOK | BER | LER | STO | TOR | ESK | COP |
|---------|-------------|-------------|--------------|--------------|--------------|--------------|--------------|--------------|--------------|--------------|
| SOD | | 0.86 | -0.57 | 0.68 | 0.59 | -0.27 | 0.59 | 0.69 | 0.27 | 0.48 |
| LUL | 0.90 | | -0.73 | 0.77 | 0.76 | -0.23 | 0.70 | 0.66 | 0.43 | 0.70 |
| REY | -0.28 | -0.24 | | -0.47 | -0.60 | 0.08 | -0.50 | -0.27 | -0.67 | -0.65 |
| JOK | 0.89 | 0.92 | -0.27 | | 0.60 | -0.53 | 0.92 | 0.92 | 0.22 | 0.77 |
| BER | 0.55 | 0.60 | -0.45 | 0.55 | | -0.08 | 0.54 | 0.49 | 0.48 | 0.56 |
| LER | 0.28 | 0.37 | -0.02 | 0.43 | 0.38 | | -0.56 | -0.53 | 0.15 | -0.36 |
| STO | 0.85 | 0.87 | -0.40 | 0.96 | 0.58 | 0.31 | | 0.81 | 0.27 | 0.86 |
| TOR | 0.83 | 0.85 | -0.16 | 0.91 | 0.34 | 0.30 | 0.82 | | 0.05 | 0.64 |
| ESK | 0.36 | 0.33 | -0.85 | 0.39 | 0.59 | 0.17 | 0.54 | 0.12 | | 0.57 |
| COP | 0.66 | 0.74 | -0.61 | 0.80 | 0.63 | 0.33 | 0.88 | 0.60 | 0.71 | |

TABLE 5. Correlation between the residual of observed and model simulated atmospheric transmittance at different stations. The lower left half of the table represents the summer season (JJA) and the upper right half represents the spring season (MAM). Boldface font denotes correlation coefficients that are statistically significant at the 95% level ($p < 0.05$). The statistical significance is estimated using a two-tailed Student's t test.

| Station | SOD | LUL | REY | JOK | BER | LER | STO | TOR | ESK | COP |
|---------|-------------|-------------|-------|-------------|-------|-------|-------------|-------------|-------|-------------|
| SOD | | 0.49 | -0.13 | 0.43 | 0.18 | 0.16 | 0.38 | 0.43 | 0.02 | 0.03 |
| LUL | 0.54 | | -0.11 | 0.43 | 0.30 | 0.08 | 0.41 | 0.21 | -0.01 | 0.11 |
| REY | 0.06 | -0.17 | | -0.21 | -0.31 | -0.03 | -0.17 | -0.00 | 0.18 | -0.04 |
| JOK | 0.64 | 0.56 | -0.11 | | 0.34 | -0.17 | 0.59 | 0.68 | 0.18 | 0.04 |
| BER | 0.05 | 0.29 | -0.50 | 0.40 | | 0.11 | 0.35 | 0.35 | 0.19 | 0.09 |
| LER | 0.11 | -0.01 | -0.30 | 0.06 | 0.14 | | 0.03 | 0.01 | 0.39 | 0.42 |
| STO | 0.47 | 0.49 | -0.31 | 0.47 | 0.21 | 0.30 | | 0.51 | 0.29 | 0.44 |
| TOR | 0.35 | 0.36 | -0.24 | 0.69 | 0.32 | 0.30 | 0.56 | | 0.25 | 0.19 |
| ESK | 0.15 | 0.13 | -0.04 | 0.20 | 0.19 | 0.21 | 0.28 | 0.16 | | 0.49 |
| COP | 0.27 | 0.46 | -0.31 | 0.46 | 0.21 | 0.48 | 0.56 | 0.52 | 0.44 | |

residual brightening of approximately $+5.0\% \text{ decade}^{-1}$ ($\approx +9 \text{ W m}^{-2} \text{ decade}^{-1}$) during the summer of 1986–2007 is statistically significant at the 95% level. However, the negative residual Tr trends before 1986 are not significant, either in the shorter period 1972–86 (see Table 6) or the extended period (1956–86; not shown in the table).

For the individual stations, we focus the trend analysis on the period 1965–2007 for which the majority of stations have available observations (see Table 1). The trends discussed in the text are not shown here but can be seen in the supplementary material (Figs. S1 and S2). At the majority of the individual sites, the observed transmittance has no statistically significant

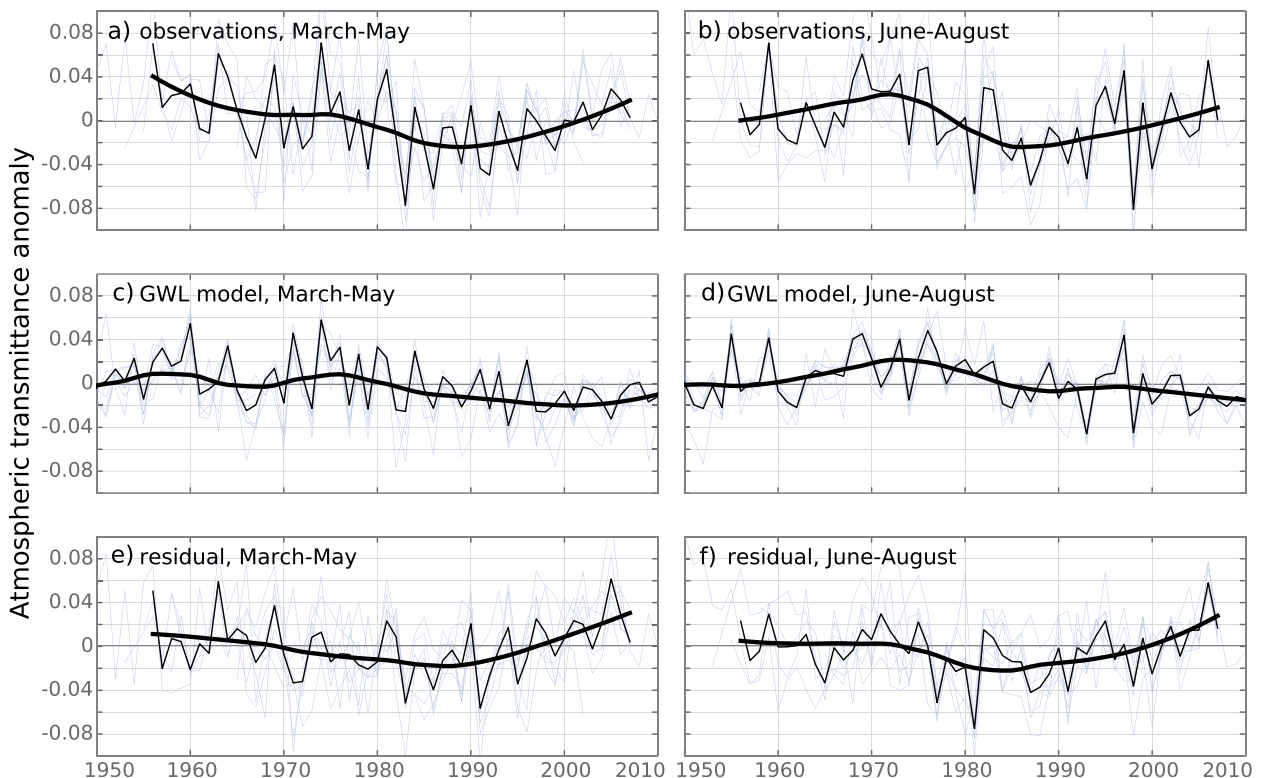


FIG. 7. Regionally averaged time series of (top) observed, (middle) modeled, and (bottom) residual (observed – modeled) atmospheric transmittance, for (left) spring and (right) summer. The thinner blue lines represent the seasonal average transmittance for individual stations (Sodankyla, Lulea, Jokioinen, Bergen, Stockholm, Toravere, Eskdalemuir, and Copenhagen), the thin black line is a regional average and the thicker black line is a smoothed regional average (Lowess curve with a window width corresponding to 30 yr).

TABLE 6. Trend analysis of observed, modeled and residual regional average transmittance for the spring (MAM) and summer (JJA) season. The trend magnitude per decade is reported in absolute terms and relative to the average observed transmittance (% decade⁻¹). The regional average transmittance is calculated based on all stations (see Fig. 1) except Lerwick and Reykjavik. The rate of change is calculated by linear regression and the statistical significance is estimated using the Mann–Kendall test. The *p* value of the Mann–Kendall test indicates that the probability with which we can reject the null hypothesis of no change. Trends that are statistically significant at the 95% level (i.e., *p* < 0.05) are marked in boldface. Trends are estimated for the periods 1956–89, 1989–2007, and 1956–2007 for spring and 1956–72, 1972–86, and 1986–2007 for summer. The periods were selected based on the maximum and minimum points of the smoothed observed transmittance time series in Figs. 7a and 7b.

| | Absolute | Relative | <i>p</i> | Absolute | Relative | <i>p</i> | Absolute | Relative | <i>p</i> |
|--------------|---------------|--------------|-------------|---------------|--------------|--------------|---------------|--------------|--------------|
| MAM | | 1956–89 | | | 1989–2007 | | | 1956–2007 | |
| Observations | −0.014 | −3.1% | 0.01 | +0.025 | +5.6% | 0.002 | −0.005 | −1.1% | 0.09 |
| GWL model | −0.006 | −1.4% | 0.14 | −0.002 | −0.44% | 0.89 | −0.006 | −1.3% | 0.005 |
| Residual | −0.008 | −1.8% | 0.03 | +0.027 | +6.1% | 0.01 | +0.0009 | +0.2% | 0.54 |
| JJA | | 1956–72 | | | 1972–86 | | | 1986–2007 | |
| Observations | +0.019 | +4.3% | 0.20 | −0.036 | −8.2% | 0.17 | +0.018 | +4.0% | 0.10 |
| GWL model | +0.013 | +3.0% | 0.08 | −0.020 | −4.6% | 0.08 | −0.004 | −1.0% | 0.57 |
| Residual | +0.006 | +1.3% | 0.30 | −0.016 | −3.6% | 0.20 | +0.022 | +5.0% | 0.001 |

trends, but there are mutual tendencies within the region.

In spring, observed *Tr* decreased during the period 1965–89 at all stations but two (Reykjavik and Toravere), but the negative trend is statistically significant only in Sodankyla. After 1989, the observed *Tr* increases at 8 of 10 sites, statistically significantly at five of them. At most sites, the magnitude of the brightening after 1989 is also much stronger than the previous *Tr* decrease during 1965–89. Reykjavik and Copenhagen experienced statistically significant negative transmittance trends after 1989.

In summer, the early 1970s maximum seen in the regional average transmittance (Figs. 7b,d) is also a distinct feature at many of the individual sites (Fig. 4). A peak and following decrease in observed *Tr* is found in 8 of 10 stations (not Reykjavik and Bergen), but the trend for 1972–86 is statistically significant only in Stockholm where the decrease is also remarkably strong (−15% decade⁻¹). After 1986, the observed transmittance increases at all sites except Lerwick and Reykjavik, but again the trend is only statistically significant in Stockholm.

The model simulated transmittance decreases from 1965–2007 at the sites in Scandinavia, Finland, and Estonia, statistically significant at several sites (five in summer, two in spring). On shorter time scales, the modeled transmittance trends are not strong enough to be statistically significant. However, at most sites the observed transmittance trends are weak to begin with and partially reproduced by the GWL models, resulting in a residual transmittance without any strong or statistically significant changes before 1990. The notable exceptions are Stockholm, Sodankyla, and (in summer but not spring) Eskdalemuir, where stronger *Tr* changes occur and the GWL models explain only a minor portion of the observed *Tr* trends. A similar spatial pattern of

transmittance trends is found in both the observed and modeled transmittance in spring during the period 1965–89: negative transmittance trends (weak and mostly nonsignificant) in Scandinavia and the United Kingdom, and a positive transmittance trend in Reykjavik.

The observed brightening after 1990 is not reproduced by any of the GWL models. The residual *Tr* trends are positive at all stations except Reykjavik and (in spring, not summer) Copenhagen, and statistically significant at 4 of the 10 sites. The residual transmittance trends from the late 1980s to 2007 range from around +1% to over +10% decade⁻¹ in mainland northern Europe and the United Kingdom, the magnitude depending on site, season, and the exact period considered.

5. Discussion

a. Interpretation of the GWL models and residual transmittance

The results of the permutation test—that the GWL models are statistically distinguishable from randomized models—established that the GWL contain atmospheric circulation information relevant to the atmospheric transmittance of SW radiation (section 4a, Table 2). Furthermore, the relationship between atmospheric transmittance and the synoptic weather patterns is relatively stable throughout the calibration period, as demonstrated by the jackknife generated confidence intervals (section 4a, Figs. 3 and 4). We conclude that for northern Europe, the GWL model methodology developed in Parding et al. (2016) can be used to assess the connection between large-scale weather patterns and SW irradiance.

The spatial homogeneity of the modeled atmospheric transmittance (section 4b, Table 4) supports the

interpretation of the GWL models as a radiative effect of large-scale weather patterns. The influence of atmospheric circulation on SW irradiance is expected to have a large-scale signature related to cloud patterns (Chiacchio and Vitolo 2012). Previous studies suggest that atmospheric circulation patterns influence SW irradiance primarily via the redistribution of clouds (Sanchez-Lorenzo et al. 2009; Chiacchio and Wild 2010). However, the atmospheric circulation could also modulate the transport and deposition of aerosols via wind and precipitation. The spatial heterogeneity of the residual transmittance (observed Tr minus modeled Tr) indicates that the processes that influence the residual act on smaller spatial scales and are independent of large-scale weather patterns. The residual Tr variability may include radiative effects of aerosol emissions as well as small-scale meteorological phenomena that are not represented by the GWL. Nevertheless, an influence of aerosols on the atmospheric circulation cannot be excluded (Sanchez-Lorenzo et al. 2009; Chiacchio et al. 2011; Allen and Sherwood 2011). This means that a total separation between “natural” SW irradiance variability and aerosol effects cannot be guaranteed even if the GWL models were to perfectly represent the radiative effects of large-scale weather patterns. More convective cloud formation that is independent of large-scale weather patterns is expected in summer and this may explain the relatively poorer performance of the GWL models in summer compared to spring.

b. Global dimming and brightening

The observed, GWL modeled, and residual transmittance presented in this study suggest that while the large-scale atmospheric circulation causes considerable interannual and decadal SW irradiance variations, there is also room for other factors such as varying atmospheric aerosol emissions, humidity changes, or convective cloud formation. In particular, the observations show a strong brightening in recent decades that is even more pronounced when considering the weather-pattern-independent residual transmittance. The recent brightening is stronger and more spatially homogeneous than the Tr changes seen before 1990. These results are in line with the results of Stjern et al. (2009), who reported a significant brightening since the 1980s in northern Europe, which in many stations could not be explained by cloud cover changes. A similar increase in SW irradiance has occurred across Europe in spring and summer since the 1980s, although the brightening in northern Europe is stronger than the European average (Sanchez-Lorenzo et al. 2015). Reduced atmospheric aerosol loadings are a likely explanation of the recent

brightening. The emission of sulfuric aerosols in Europe reached a maximum in the 1980s and has since decreased because of stricter air quality controls and environmental regulation of household, industrial, and transportation-related fossil fuel burning (Streets et al. 2006). Climate model simulations show that the recent decline in atmospheric aerosol can explain the recent brightening (Turnock et al. 2015; Nabat et al. 2014), but the simulations predict a smaller brightening in northern Europe than in central Europe while observations show the opposite. The apparent discrepancy could be due to issues with the aerosol histories or climate models, but it is also possible that the aerosol brightening in northern Europe is enhanced by local meteorological processes influencing the cloud cover and humidity.

From the 1950s to 1980s, the regional average transmittance in spring shows a significant dimming, but there are large variations between stations and trends are significant only for a few stations. A case study of cloud and solar observations in Bergen (Parding et al. 2014) showed that the decreasing SW irradiance during this period could be explained by an increasing cloud cover, in particular of low clouds. (Stjern et al. 2009) reported that in some months and stations, the observed SW irradiance trends in northern Europe were accompanied by cloud cover trends of the opposite sign. These results indicate that in most stations in northern Europe, the cloud variations have had a considerably stronger effect on SW irradiance during this period than aerosol emissions. Given the strong aerosol signal in the recent brightening, one might expect an equally strong dimming signal in the period of increasing aerosol emissions. The reason for the lack of a pronounced dimming in the regional average transmittance could be that the increase in aerosol loading started earlier than the majority of the SW irradiance observations.

c. Radiative effects of cyclonic and anticyclonic weather patterns over northern Europe

In Parding et al. (2016), two groups of weather patterns were identified among the GWL that had a strong connection to the SW irradiance in Bergen. These synoptic weather patterns were characterized by low or high pressure centers in the vicinity of the station but also importantly the wind flow in over the topography because orographic clouds and precipitation are important in this area. For the larger northern European region, we can in a similar way identify 14 weather patterns that explain more than 90% of the variability in the regional average Tr models (Figs. 7b,d). The weather patterns that have a strong influence on the SW irradiance in

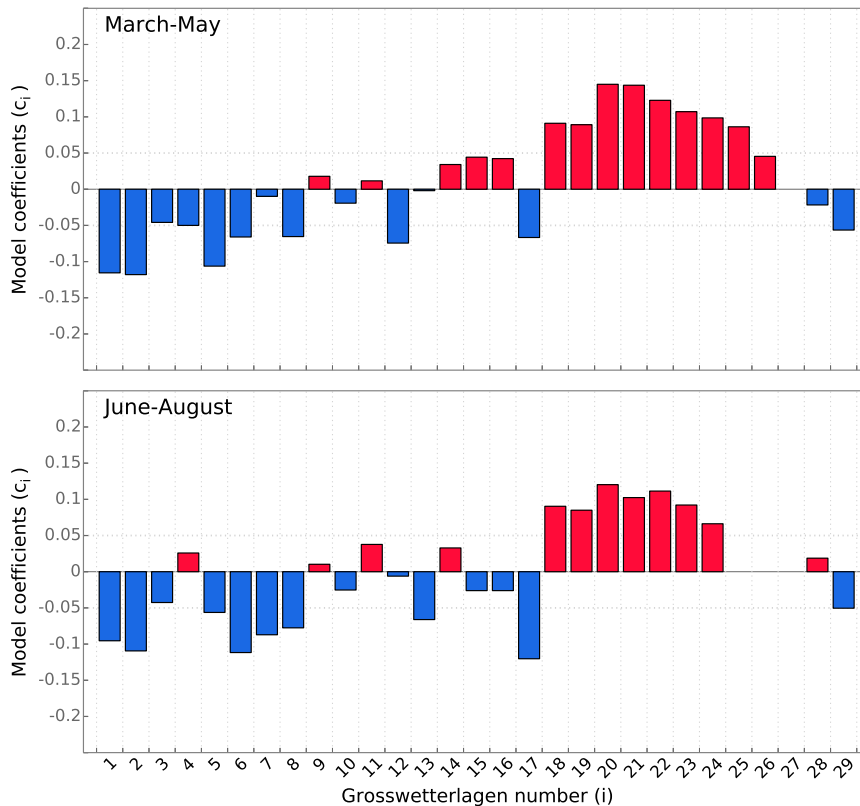


FIG. 8. Coefficients of the regional average GWL models displayed in Fig. 7. The coefficients c_i represent the transmittance anomaly associated with each weather patterns GWL i ($i = 1-29$). Weather patterns with positive coefficients (e.g., GWL 18–25) are associated with anomalously high SW irradiance in northern Europe while GWL with negative coefficients (e.g., GWL 1, 2) are characterized by lower than average SW irradiance.

northern Europe are selected based on having coefficients larger than ± 0.05 for both spring and summer (Fig. 8), and can be divided into two groups,

$$\begin{aligned} \text{GWL}(+) &= \text{GWL } 18-24 \text{ and} \\ \text{GWL}(-) &= \text{GWL } 1, 2, 5, 6, 8, 17, \text{ and } 29, \end{aligned}$$

depending on whether they have a positive or negative contribution to the atmospheric transmittance anomalies in northern Europe. The average SLP maps associated with the GWL(+) and GWL(-) weather patterns are displayed in Fig. 2.

The weather patterns associated with positive transmittance anomalies in northern Europe, GWL(+), are characterized by high sea level pressure over Scandinavia and the Baltic region (GWL 18–24; Fig. 2). The GWL associated with negative transmittance anomalies, GWL(-), instead tend to have low SLP over the North Atlantic and northwestern Europe. The effect of the weather patterns GWL(+) and GWL(-) on SW irradiance can be explained in terms of the expected cloud patterns: reduced humidity and cloud formation

in the vicinity of anticyclonic weather patterns and increased cloudiness expected around cyclonic weather patterns.

The variations of the weather patterns GWL(+) and GWL(-) in years of maximum and minimum observed transmittance demonstrate how the weather patterns contribute to the observed transmittance variability. In anomalously sunny years (the top 10th percentile of observed regionally averaged atmospheric transmittance) the frequency of the anticyclonic weather patterns GWL(+) is higher than usual. For example, the frequency of GWL 20 is usually around 4% in both spring and summer, but in the anomalously sunny years they occur more than twice as often (12% in spring, 10% in summer). The increased frequency of GWL 20 alone explains more than 20% of the increased transmittance in the positive peak years. A reduced frequency of the GWL associated with cyclonic weather patterns, GWL(-), also contributes to the positive transmittance anomalies. In the low transmittance years (lowest 10th percentile of observed Tr), the conditions are the opposite:

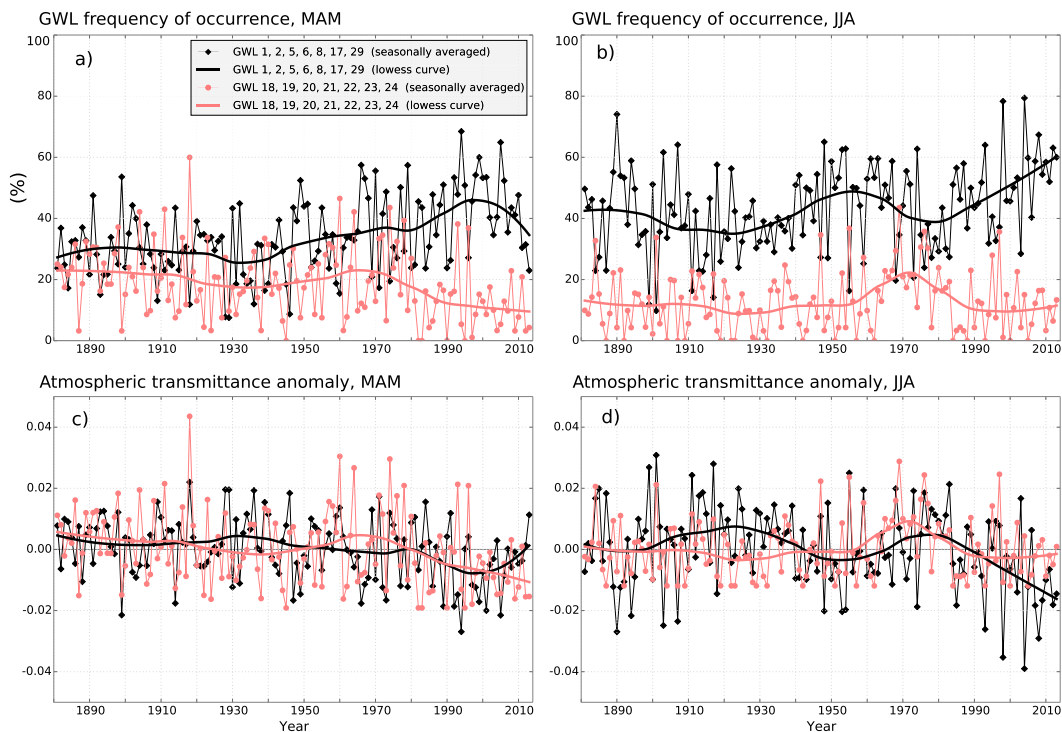


FIG. 9. (a),(b) The seasonally averaged frequency of occurrence of two groups of weather patterns, GWL 1, 2, 5, 6, 8, 17, and 29 (black lines and markers), which are characterized by low sea level pressure over the North Atlantic and northern Europe, and GWL 18, 19, 20, 21, 22, 23, and 24 (pink lines and markers) with high sea level pressure centers over Scandinavia and the Baltic region (see SLP maps in Fig. 2), for (left) spring and (right) summer. (c),(d) The atmospheric transmittance anomalies associated with these weather patterns, estimated by the empirical GWL models (see section 3a). The seasonally averaged time series are shown as markers connected by thin lines and the smoothed seasonal Lowess curves as thicker lines.

anticyclonic weather patterns GWL(+) occur with less frequency and cyclonic weather patterns GWL(−) occur more often.

d. Trends of cyclonic and anticyclonic weather patterns over northern Europe

In spring, the occurrence of the cyclonic weather patterns GWL(−) increases from a decadal average frequency of 28% in the 1950s to 41% in the 1990s, with the strongest change occurring during the 1980s and 90s (Fig. 9a). During the same period, the frequency of the anticyclonic weather patterns GWL(+) declines, from 25% in the 1950s to 18% in the 1990s. The transmittance anomalies associated with these changes, as estimated by the regional average GWL model components of GWL(−) and GWL(+), are displayed in Fig. 9c. Based on the GWL models, the weather pattern shifts described above causes a 3% point reduction of the average northern European transmittance from the 1950s to the 1990s in spring. Approximately two-thirds of the modeled Tr change during this period can be attributed to the increasing frequency of cyclonic weather patterns

and one-third to the decreasing occurrence of anticyclonic patterns.

In summer, the Tr maximum in the early 1970s can be traced to a temporary rise in anticyclonic weather patterns GWL(+) and a smaller concurrent decline in cyclonic weather patterns GWL(−) (Fig. 9b). Before the local Tr maximum, the occurrence of the anticyclonic patterns GWL(+) increased from an average frequency of 14% in the 1940s to 22% during the period 1965–1974. The frequency of the cyclonic weather patterns (Figs. 2a–f) decreased by only 3% points, from 42% in the 1940s to 39% during 1965–74. The total Tr change associated with the GWL variations described above is +3.1 percentage points, four-fifths of which can be attributed to the anticyclonic weather patterns. After the Tr maximum, the anticyclonic weather patterns decreased, returning to an average frequency of 16% in the 1990s, and cyclonic weather patterns increased to 42% in the same period. The GWL changes from the 1970s to the 1990s are associated with a total modeled Tr change of −3.2% points, more than two-thirds attributable to the decreasing

frequency of the anticyclonic weather patterns $\text{GWL}(+)$ (Fig. 9d).

e. The Iceland–Scandinavia dipole pattern

Because the GWL are defined to describe the weather patterns in central Europe, the classification may not be a relevant description of the large-scale circulation at faraway sites such as Reykjavik in Iceland (see map in Fig. 1). That said, the observed anticorrelation between Tr in Reykjavik and the other northern European sites is reproduced by the GWL models (section 4b, Tables 3 and 4), which suggests that it is related to aspects of the atmospheric circulation that are represented by the GWL . A comparison of the individual GWL models show the anticorrelation is connected to GWL with coefficients [c_i in Eq. (1)] of the opposite sign in the Reykjavik GWL model compared to the other stations (see Figs. S3 and S4 in the supplementary material). The coefficients represent the local transmittance anomalies associated with each weather pattern, so the opposite sign coefficients can be interpreted as weather patterns with opposing effects at Reykjavik and mainland Europe (e.g., anticyclonic over Iceland and cyclonic over Scandinavia).

In Reykjavik, the previously defined groups of weather patterns have the opposite radiative effect compared to the other stations (Figs. S3 and S4): The Scandinavian anticyclonic weather patterns $\text{GWL}(+)$ are associated with negative transmittance anomalies and the North Atlantic cyclonic $\text{GWL}(-)$ weather patterns with anomalously sunny conditions in Reykjavik. Reykjavik tends to fall outside of the pressure zone that includes the other sites (e.g., for GWL 18–24 Reykjavik is not in the high pressure zone over Scandinavia), which explains the anticorrelation between SW irradiance in Reykjavik and the other northern European sites.

f. Multidecadal climate variability in the North Atlantic

Changes in anticyclonic and cyclonic weather patterns over northern Europe in summer may be connected to shifts in the North Atlantic storm tracks. The dominant mode of interannual summer storm track variability, identified by Dong et al. (2013) as the first principal component (PC1) of the summer storm density, is characterized by a meridional shift between two preferred paths. When the storm track is shifted southward, the preferred path of the cyclonic weather systems is zonally elongated over the United Kingdom and into northwestern Europe, resulting in wet summers and a reduced frequency of blocking anticyclonic systems in northwestern Europe. The northward shifted storm track, on the other hand, lets the cyclonic systems enter

the Arctic without passing the United Kingdom or Scandinavia, and is associated with increased blocking over northwestern Europe. The storm track shifts have been connected to the summer North Atlantic Oscillation (NAO), the positive (negative) phase of the index being associated with a southward (northward) shifted storm track and increased (reduced) cloud cover and precipitation in summer (Dong et al. 2013; Folland et al. 2009; Knight et al. 2005). The Tr maximum in the early 1970s coincides with a period of northward shifted storm tracks (Fig. 1b of Dong et al. 2013) and high positive values of the NAO index. This suggests that the shifts of the North Atlantic storm tracks in summer have a notable influence on the radiative climate in northern Europe. The shifts in North Atlantic storm tracks and multidecadal variations of the climate in northwestern Europe have furthermore been connected to the North Atlantic sea surface temperatures (SSTs) (Knight et al. 2005; Wilson et al. 2009; Sutton and Hodson 2005; Woollings et al. 2012). Climate model simulations predict a northward shift in midlatitude storm tracks as a response to a continued increase in greenhouse gases (Woollings et al. 2012; Yin 2005), which may have considerable effect on the SW irradiance climate in northern Europe in the future.

The North Atlantic storm tracks could also explain the observed anticorrelation between Tr in Iceland and mainland northern Europe. When the storm track is shifted south, eastward traveling cyclones tend to pass south of Iceland on their way to northern Europe (Dong et al. 2013). The north-shifted storm track instead has cyclones entering the Arctic via Iceland but north of the United Kingdom and Scandinavia. In both cases, one would expect opposite transmittance effects in Iceland and mainland Europe: reduced Tr in regions with increased cyclonic activity and increased Tr where the cyclones do not pass.

6. Summary and conclusions

We construct empirical models of the normalized surface SW irradiance (atmospheric transmittance, Tr) using the Grosswetterlagen (GWL), a daily classification of European synoptic weather patterns. The GWL models represent the portion of transmittance variability that is driven by large-scale atmospheric circulation. Thus this procedure enables us to quantify the contribution of atmospheric circulation to SW irradiance. The transmittance obtained from GWL models explains 22%–58% of the observed interannual transmittance variability in summer and 3%–42% in spring. The residual (observed minus modeled) transmittance can be interpreted as the portion of Tr associated with other

factors that influence SW irradiance, such as meteorological processes on smaller spatial scales or varying atmospheric aerosol loads.

The most prominent and spatially homogeneous feature of the weather-pattern-independent transmittance is the strong residual brightening seen at most of the northern European sites from the late 1980s to the 2000s. In mainland northern Europe, the residual brightening ranges from +1% decade⁻¹ to over +10% decade⁻¹. We speculate that the change in this period is caused by decreasing aerosol emissions, which is in line with the literature (Streets et al. 2006; Wild 2012; Nabat et al. 2014; Turnock et al. 2015).

On average, approximately 50%–60% of the observed decadal-scale trends of transmittance in northern Europe before 1990 can be explained by atmospheric circulation (Table 6). At most individual sites, the decadal-scale trends of observed transmittance before 1990 are small, not statistically significant, and generally in agreement with the GWL modeled transmittance. We conclude that the strong weather-pattern-independent dimming is confined to a few stations—most notably Sodankyla and Stockholm—and not a common feature in northern Europe.

The transmittance variations before 1990 can be traced to shifts in specific weather pattern types. We find changes of the frequency of weather patterns as follows: In spring, the occurrence of weather patterns with low SLP over the North Atlantic and northern Europe increased by 13% points from the 1950s to the 1990s. During the same period, the frequency of weather patterns characterized by high SLP over northern Europe decreased by 7% points. The GWL models indicate that these weather pattern changes contributed to the dimming tendencies from the 1950s to the 1990s seen at many sites in spring. In summer, the transmittance peaks in the early 1970s are linked to a temporary increase in high SLP patterns (~+8%) and a reduction of low SLP patterns (~-3%). We see a possible connection between the observed weather pattern changes described above and the south–north shifts of the North Atlantic storm track during the summer (Dong et al. 2013).

At many northern European sites, observed dimming tendencies from the 1950s to the 1980s can be explained by increasing cloud cover in spring and summer months, as seen in previous studies (Stjern et al. 2009). Based on the evidence outlined in this paper, we conclude that the cloud-induced dimming in northern Europe before 1990 is connected to atmospheric circulation rather than indirect aerosol effects. The changing weather patterns are not expected to have the same influence on the radiative climate in other parts of Europe or the rest of the world. The relative importance of atmospheric

circulation and other factors influencing SW irradiance appears to vary from site to site and period to period. Therefore, a regional or local approach may be preferable to global or continental scales when studying the causes of global dimming and brightening.

Acknowledgments. The authors thank the reviewers for their constructive comments and thoughtful suggestions.

REFERENCES

- Allen, R., and S. C. Sherwood, 2011: The impact of natural versus anthropogenic aerosols on atmospheric circulation in the Community Atmosphere Model. *Climate Dyn.*, **36**, 1959–1978, doi:10.1007/s00382-010-0898-8.
- Baur, F., P. Hess, and H. Nagel, 1944: Kalender der Großwetterlagen Europas 1881–1939. PIK Tech. Rep. 119, 146 pp.
- Chiacchio, M., and M. Wild, 2010: Influence of NAO and clouds on long-term seasonal variations of surface solar radiation in Europe. *J. Geophys. Res.*, **115**, D00D22, doi:10.1029/2009JD012182.
- , and R. Vitolo, 2012: Effect of cloud cover and atmospheric circulation patterns on the observed surface solar radiation in Europe. *J. Geophys. Res.*, **117**, D18207, doi:10.1029/2012JD017620.
- , T. Ewen, M. Wild, and E. Arabini, 2010: Influence of climate shifts on decadal variations of surface solar radiation in Alaska. *J. Geophys. Res.*, **115**, D00D21, doi:10.1029/2009JD012533.
- , —, —, M. Chin, and T. Diehl, 2011: Decadal variability of aerosol optical depth in Europe and its relationship to the temporal shift of the North Atlantic Oscillation in the realm of dimming and brightening. *J. Geophys. Res.*, **116**, D02108, doi:10.1029/2010JD014471.
- Dong, B., R. T. Sutton, T. Woollings, and K. Hodges, 2013: Variability of the North Atlantic summer storm track: Mechanisms and impacts on European climate. *Environ. Res. Lett.*, **8**, 034037, doi:10.1088/1748-9326/8/3/034037.
- Folini, D., and M. Wild, 2011: Aerosol emissions and dimming/brightening in Europe: Sensitivity studies with ECHAM5-HAM. *J. Geophys. Res.*, **116**, D21104, doi:10.1029/2011JD016227.
- Folland, C. K., J. Knight, H. W. Linderholm, D. Fereday, S. Ineson, and J. W. Hurrell, 2009: The summer North Atlantic Oscillation: Past, present, and future. *J. Climate*, **22**, 1082–1103, doi:10.1175/2008JCLI2459.1.
- Fröhlich, C., 2009: Evidence of a long-term trend in total solar irradiance. *Astron. Astrophys.*, **501**, L27–L30, doi:10.1051/0004-6361/200912318.
- Gilgen, H., and A. Ohmura, 1999: The Global Energy Balance Archive. *Bull. Amer. Meteor. Soc.*, **80**, 831–850, doi:10.1175/1520-0477(1999)080<0831:TGEBA>2.0.CO;2.
- , M. Wild, and A. Ohmura, 1998: Means and trends of shortwave irradiance at the surface estimated from Global Energy Balance Archive data. *J. Climate*, **11**, 2042–2061, doi:10.1175/1520-0442-11.8.2042.
- , A. Roesch, M. Wild, and A. Ohmura, 2009: Decadal changes in shortwave irradiance at the surface in the period from 1960 to 2000 estimated from Global Energy Balance Archive data. *J. Geophys. Res.*, **114**, D00D08, doi:10.1029/2008JD011383.
- Hinkelman, L. M., P. W. Stackhouse, B. A. Wielicki, T. Zhang, and S. R. Wilson, 2009: Surface insolation trends from satellite and

- ground measurements: Comparisons and challenges. *J. Geophys. Res.*, **114**, D00D20, doi:10.1029/2008JD011004.
- Iqbal, M., 1983: *An Introduction to Solar Radiation*. 1st ed. Academic Press, 310 pp.
- Jacobson, M. Z., and M. A. Delucchi, 2011: Providing all global energy with wind, water, and solar power, Part I: Technologies, energy resources, quantities and areas of infrastructure, and materials. *Energy Policy*, **39**, 1154–1169, doi:10.1016/j.enpol.2010.11.040.
- Kanamitsu, M., W. Ebisuzaki, J. Woollen, S.-K. Yang, J. J. Hnilo, M. Fiorino, and G. L. Potter, 2002: NCEP–DOE AMIP-II Reanalysis (R-2). *Bull. Amer. Meteor. Soc.*, **83**, 1631–1643, doi:10.1175/BAMS-83-11-1631.
- Kendall, M. G., 1962: *Rank Correlation Methods*. 3rd ed. Hafner, 199 pp.
- Knight, J. R., R. J. Allan, C. K. Folland, M. Vellinga, and M. E. Mann, 2005: A signature of persistent natural thermohaline circulation cycles in observed climate. *Geophys. Res. Lett.*, **32**, L20708, doi:10.1029/2005GL024233.
- Kopp, G., and J. L. Lean, 2011: A new, lower value of total solar irradiance: Evidence and climate significance. *Geophys. Res. Lett.*, **38**, L01706, doi:10.1029/2010GL045777.
- Liepert, B. G., 2002: Observed reductions of surface solar radiation at sites in the United States and worldwide from 1961 to 1990. *Geophys. Res. Lett.*, **29**, 1421, doi:10.1029/2002GL014910.
- , and A. Romanou, 2005: Global dimming and brightening and the water cycle. *Bull. Amer. Meteor. Soc.*, **86**, 622–623.
- , J. Feichter, U. Lohmann, and E. Roeckner, 2004: Can aerosols spin down the water cycle in a warmer and moister world? *Geophys. Res. Lett.*, **31**, L06207, doi:10.1029/2003GL019060.
- Liley, J. B., 2009: New Zealand dimming and brightening. *J. Geophys. Res.*, **114**, D00D10, doi:10.1029/2008JD011401.
- Long, C. N., E. G. Dutton, J. A. Augustine, W. Wiscombe, M. Wild, S. A. McFarlane, and C. J. Flynn, 2009: Significant decadal brightening of downwelling shortwave in the continental United States. *J. Geophys. Res.*, **114**, D00D06, doi:10.1029/2008JD011263.
- Mercado, L. M., N. Bellouin, S. Sitch, O. Boucher, C. Huntingford, M. Wild, and P. M. Cox, 2009: Impact of changes in diffuse radiation on the global land carbon sink. *Nature*, **458**, 1014–1017, doi:10.1038/nature07949.
- Murphy, D. M., S. Solomon, R. W. Portmann, K. H. Rosenlof, P. M. Forster, and T. Wong, 2009: An observationally based energy balance for the Earth since 1950. *J. Geophys. Res.*, **114**, D17107, doi:10.1029/2009JD012105.
- Nabat, P., S. Somot, M. Mallet, A. Sanchez-Lorenzo, and M. Wild, 2014: Contribution of anthropogenic sulfate aerosols to the changing Euro-Mediterranean climate since 1980. *Geophys. Res. Lett.*, **41**, 5605–5611, doi:10.1002/2014GL060798.
- Norris, J. R., and M. Wild, 2007: Trends in aerosol radiative effects over Europe inferred from observed cloud cover, solar “dimming,” and solar “brightening.” *J. Geophys. Res.*, **112**, D08214, doi:10.1029/2006JD007794.
- Ohvri, H., and Coauthors., 2009: Global dimming and brightening versus atmospheric column transparency, Europe, 1906–2007. *J. Geophys. Res.*, **114**, D00D12, doi:10.1029/2008JD010644.
- Parding, K., J. A. Olseth, K.-F. Dagestad, and B. G. Liepert, 2014: Decadal variability of clouds, solar radiation and temperature at a high-latitude coastal site in Norway. *Tellus*, **66B**, 25897, doi:10.3402/tellusb.v66.25897.
- , —, B. G. Liepert, and K.-F. Dagestad, 2016: Influence of atmospheric circulation patterns on local cloud and solar variability in Bergen, Norway. *Theor. Appl. Climatol.*, doi:10.1007/s00704-015-1517-8, in press.
- Ruckstuhl, C., and J. Norris, 2009: How do aerosol histories affect solar “dimming” and “brightening” over Europe?: IPCC-AR4 models versus observations. *J. Geophys. Res.*, **114**, D00D04, doi:10.1029/2008JD011066.
- Russak, V., 1990: Trends of solar radiation, cloudiness and atmospheric transparency during recent decades in Estonia. *Tellus*, **42B**, 206–210, doi:10.1034/j.1600-0889.1990.t01-1-00006.x.
- , 2009: Changes in solar radiation and their influence on temperature trend in Estonia (1955–2007). *J. Geophys. Res.*, **114**, D00D01, doi:10.1029/2008JD010613.
- Sanchez-Lorenzo, A., J. Calbó, and J. Martin-Vide, 2008: Spatial and temporal trends in sunshine duration over western Europe (1938–2004). *J. Climate*, **21**, 6089–6098, doi:10.1175/2008JCLI2442.1.
- , —, M. Brunetti, and C. Deser, 2009: Dimming/brightening over the Iberian Peninsula: Trends in sunshine duration and cloud cover and their relations with atmospheric circulation. *J. Geophys. Res.*, **114**, D00D09, doi:10.1029/2008JD011394.
- , M. Wild, and J. Trentmann, 2013: Validation and stability assessment of the monthly mean CM SAF surface solar radiation dataset over Europe against a homogenized surface dataset (1983–2005). *Remote Sens. Environ.*, **134**, 355–366, doi:10.1016/j.rse.2013.03.012.
- , —, M. Brunetti, J. A. Guijarro, M. Z. Hakuba, J. Calbó, S. Mystakidis, and B. Bartok, 2015: Reassessment and update of long-term trends in downward surface shortwave radiation over Europe (1939–2012). *J. Geophys. Res. Atmos.*, **120**, 9555–9569, doi:10.1002/2015JD023321.
- Stanhill, G., and S. Cohen, 2001: Global dimming: A review of the evidence for a widespread and significant reduction in global radiation with discussion of its probable causes and possible agricultural consequences. *Agric. For. Meteorol.*, **107**, 255–278, doi:10.1016/S0168-1923(00)00241-0.
- Stjern, C. W., J. E. Kristjánsson, and A. W. Hansen, 2009: Global dimming and global brightening—An analysis of surface radiation and cloud cover data in northern Europe. *Int. J. Climatol.*, **29**, 643–653, doi:10.1002/joc.1735.
- Streets, D. G., Y. Wu, and M. Chin, 2006: Two-decadal aerosol trends as a likely explanation of the global dimming/brightening transition. *Geophys. Res. Lett.*, **33**, L15806, doi:10.1029/2006GL026471.
- Sutton, R. T., and D. L. R. Hodson, 2005: Atlantic Ocean forcing of North American and European summer climate. *Science*, **309**, 115–118, doi:10.1126/science.1109496.
- Taylor, J. R., 1997: *An Introduction to Error Analysis: The Study of Uncertainties in Physical Measurements*. University Science Books, 327 pp.
- Turnock, S. T., and Coauthors, 2015: Modelled and observed changes in aerosols and surface solar radiation over Europe between 1960 and 2009. *Atmos. Chem. Phys.*, **15**, 9477–9500, doi:10.5194/acp-15-9477-2015.
- Werner, P. C., and F.-W. Gerstengarbe, 2010: Katalog der Großwetterlagen Europas (1881–2009). PIK Rep. 119, 146 pp.
- Wild, M., 2012: Enlightening global dimming and brightening. *Bull. Amer. Meteor. Soc.*, **93**, 27–37, doi:10.1175/BAMS-D-11-00074.1.
- , and Coauthors, 2005: From dimming to brightening: Decadal changes in solar radiation at Earth’s surface. *Science*, **308**, 847–850, doi:10.1126/science.1103215.
- , A. Ohmura, and K. Makowski, 2007: Impact of global dimming and brightening on global warming. *Geophys. Res. Lett.*, **34**, L04702, doi:10.1029/2006GL028031.

- Wilson, C., B. Sinha, and R. G. Williams, 2009: The effect of ocean dynamics and orography on atmospheric storm tracks. *J. Climate*, **22**, 3689–3702, doi:[10.1175/2009JCLI2651.1](https://doi.org/10.1175/2009JCLI2651.1).
- Woollings, T., J. M. Gregory, J. G. Pinto, M. Reyers, and D. J. Brayshaw, 2012: Response of the North Atlantic storm track to climate change shaped by ocean–atmosphere coupling. *Nat. Geosci.*, **5**, 313–317, doi:[10.1038/ngeo1438](https://doi.org/10.1038/ngeo1438).
- Yang, K., B. Ding, J. Qin, W. Tang, N. Lu, and C. Lin, 2012: Can aerosol loading explain the solar dimming over the Tibetan Plateau? *Geophys. Res. Lett.*, **39**, L20710, doi:[10.1029/2012GL053733](https://doi.org/10.1029/2012GL053733).
- Yin, J. H., 2005: A consistent poleward shift of the storm tracks in simulations of 21st century climate. *Geophys. Res. Lett.*, **32**, L18701, doi:[10.1029/2005GL023684](https://doi.org/10.1029/2005GL023684).
- You, Q., A. Sanchez-Lorenzo, M. Wild, D. Folini, K. Fraedrich, G. Ren, and S. Kang, 2013: Decadal variation of surface solar radiation in the Tibetan Plateau from observations, reanalysis and model simulations. *Climate Dyn.*, **40**, 2073–2086, doi:[10.1007/s00382-012-1383-3](https://doi.org/10.1007/s00382-012-1383-3).